

Caspase-1 cleaves Bid to release mitochondrial SMAC and drive secondary necrosis in absence of GSDMD

Rosalie Heilig¹, Marisa Dilucca¹, Dave Boucher¹, Kaiwen W. Chen¹, Dora Hancz¹, Benjamin Demarco¹, Kateryna Shkarina¹ and Petr Broz^{1,*}

Affiliations:

¹Department of Biochemistry, University of Lausanne, Chemin des Boveresses 155, 1066 Epalinges, Switzerland

* Corresponding Author: Department of Biochemistry, University of Lausanne, Chemin des Boveresses 155, 1066 Epalinges, Switzerland, phone: 0041 21 692 5656, petr.broz@unil.ch

SUMMARY (198/200)

Caspase-1 activation in GSDMD-deficient cells induces a rapid form of caspase-3-dependent secondary necrosis that is licensed by caspase-1-induced Bid cleavage and the release of mitochondrial SMAC.

ABSTRACT (175/175)

1 Caspase-1 drives a lytic inflammatory cell death named pyroptosis by cleaving the pore-
2 forming cell death executor gasdermin-D (GSDMD). *Gsdmd*-deficiency however only delays
3 cell lysis, indicating that caspase-1 controls alternative cell death pathways. Here we show that
4 in absence of GSDMD caspase-1 activates apoptotic initiator and executioner caspases and
5 triggers a rapid progression into secondary necrosis. GSDMD-independent cell death required
6 direct caspase-1-driven truncation of Bid and generation of caspase-3 p19/p12 by either
7 caspase-8 or caspase-9. tBid-induced mitochondrial outer membrane permeabilization
8 (MOMP) was also required to drive SMAC release and relieve IAP inhibition of caspase-3
9 thereby allowing caspase-3 auto-processing to the fully active p17/p12 form. Our data reveal
10 that cell lysis in inflammasome-activated *Gsdmd*-deficient cells is caused by a synergistic
11 effect of rapid caspase-1-driven activation of initiator caspases-8/9 and Bid cleavage, resulting
12 in an unusually fast activation of caspase-3 and immediate transition into secondary necrosis.
13 This pathway might be advantageous for the host in counteracting pathogen-induced inhibition
14 of GSDMD, but also has implications for the use of GSDMD inhibitors in immune therapies for
15 caspase-1-dependent inflammatory disease.

16

17 INTRODUCTION

18 Inflammasomes are cytosolic signalling platforms assembled after the recognition of host- or
19 pathogen-derived danger signals by cytosolic pattern recognition receptors, such as pyrin,
20 AIM2 and members of the NLR protein family (Broz and Dixit, 2016). These complexes serve
21 as activation platforms for caspase-1, the prototypical inflammatory caspase. Active caspase-
22 1 cleaves the pro-inflammatory cytokines interleukin (IL)-1 β and IL-18 to their mature bioactive
23 form, and induces a lytic form of cell death known as pyroptosis, by processing the cell death
24 executor gasdermin-D (GSDMD) (Shi et al., 2015; Kayagaki et al., 2015). Caspase cleavage
25 at the residue D276 in mouse (D275 in human), removes the inhibitory GSDMD^{CT} and allows
26 GSDMD^{NT} to translocate to cellular membranes and form permeability pores, that disrupt ion
27 homeostasis and the electrochemical gradient (Aglietti et al., 2016; Shi et al., 2015; Ding et al.,
28 2016; Liu et al., 2016; Sborgi et al., 2016; Kayagaki et al., 2015). GSDMD is also cleaved by
29 caspase-11 in mice and by caspases-4 and -5 in humans, which are activated by the so-called
30 non-canonical inflammasome pathway in response to lipopolysaccharide (LPS) stemming from
31 infections with cytosolic Gram-negative bacteria (Shi et al., 2014; Kayagaki et al., 2011; Hagar
32 et al., 2013; Kayagaki et al., 2013). Uncontrolled inflammasome activation by gain-of-function
33 mutations in inflammasome receptors or in the context of sterile inflammatory disease has
34 been linked to a number of hereditary and acquired inflammatory diseases, such as Cryopyrin-
35 associated periodic syndrome (CAPS) Muckle-wells, but also gout, Alzheimer's disease and
36 atherosclerosis (Masters et al., 2009). It is thus of high interest to target and inhibit
37 inflammasome assembly or downstream effector processes like GSDMD pore formation and
38 IL-1 β release.

39 While *Gsdmd*-deficiency results in complete abrogation of caspase-11 (-4)-induced lytic cell
40 death, it only delays caspase-1-induced cell lysis (He et al., 2015; Kayagaki et al., 2015).
41 Caspase-1 activation in *Gsdmd*^{-/-} cells correlates with high levels of caspase-3/7 and caspase-
42 8 activity, but whether these apoptotic caspases trigger lysis of *Gsdmd*-deficient cells after
43 caspase-1 activation has not been proven (He et al., 2015), and activation of apoptotic
44 caspases has been observed to occur even in inflammasome-activated WT cells (Lamkanfi et
45 al., 2008; Sagulenko et al., 2018). The lytic death of *Gsdmd*^{-/-} cells is also in contrast to the
46 notion that apoptosis is non-lytic and thus immunologically silent. However, it is also known
47 that prolonged apoptotic caspase activity will result in apoptotic cells losing membrane
48 integrity, a process termed 'secondary necrosis'. Apoptosis is executed by caspase-3/-7, which
49 themselves are activated by either caspase-8 (extrinsic apoptosis pathway) or caspase-9
50 (intrinsic or mitochondrial apoptosis pathway). Ligation of death receptors at the plasma
51 membrane (FasR, TNFR, Trail) results in the assembly of the DISC (Death inducing signalling
52 complex) or TNFR complex IIa/b, which activate caspase-8, the initiator caspase of the
53 extrinsic pathway. In type I cells caspase-8 activity is sufficient to activate the executioner

54 caspases, while in type-II cells caspase-8 requires activation of the intrinsic pathway (Jost et
55 al., 2009). Here, caspase-8 cleaves the Bcl-2 family protein Bid to generate a truncated version
56 (tBid), which triggers Bax/Bak induced mitochondrial outer membrane permeabilization
57 (MOMP). MOMP results in the release of second mitochondria-derived activator of caspases
58 (SMAC), ATP and cytochrome C to promote intrinsic apoptosis via formation of the
59 apoptosome. This complex consists of Apoptotic Protease Activating Factor 1 (APAF1),
60 cytochrome C, ATP and caspase-9 and serves as an activation platform for caspase-9 which
61 in turn cleaves caspase-3. Apoptosis is a tightly regulated process, disturbance of the
62 equilibrium of cytosolic pool of pro- and anti-apoptotic Bcl-2 family proteins can result in
63 MOMP, apoptosis induction and cell death (Vince et al., 2018). To prevent accidental activation
64 of apoptosis, Inhibitor of Apoptosis Proteins (IAPs), in particular XIAP, suppresses caspase-3/7
65 and -9 activation by direct binding to the caspases via BIR domains (Bratton et al., 2002;
66 Takahashi et al., 1998; Roy et al., 1997; Scott et al., 2005). SMAC, that is released during
67 MOMP, antagonizes IAPs thus removing the brake on caspase auto-processing and allowing
68 full activity of the executioner caspases and apoptotic cell death (Du et al., 2000; Wilkinson et
69 al., 2004; Verhagen et al., 2000).

70 Here we investigated the mechanism that induces lytic cell death after caspase-1 activation in
71 *Gsdmd*-deficient cells. We show that cell death in *Gsdmd*^{-/-} macrophages requires caspase-
72 1, Bid-dependent mitochondrial permeabilization and the executioner caspase-3. Remarkably,
73 *Gsdmd*-deficient cells form apoptotic blebs and bodies only transiently, before shifting rapidly
74 to a necrotic phenotype that is characterized by extensive membrane ballooning.
75 Unexpectedly, we found that Bid cleavage and subsequent MOMP is driven directly by
76 caspase-1 independently of caspase-8, even though high levels of cleaved caspase-8 p18 are
77 found in inflammasome-activated *Gsdmd*-deficient cells. Upon investigating the steps
78 downstream of MOMP, we observed that knocking-out *Casp9* in *Gsdmd*^{-/-} cells had only a
79 small effect on cell death, while removing both *Casp8* and *Casp9* abrogated GSDMD-
80 independent cell death. The redundancy in caspase-8 and -9 requirement was explained by
81 the observation that either caspase was sufficient to process caspase-3 between the large and
82 small catalytic domains thereby generating the intermediate caspase-3 p19 and p12
83 fragments. Caspase-1-dependent Bid cleavage and SMAC release is then required to remove
84 IAP inhibition, thereby allowing auto-cleavage of caspase-3 to the p17/p12 fragments and full
85 caspase activation (Kavanagh et al., 2014). Thus, cell lysis in absence of GSDMD is driven by
86 the synergistic effect of both rapid caspase-1-driven activation of initiator caspases-8/-9 and
87 Bid cleavage, which results in an unusually fast activation of caspase-3 and immediate
88 transition into secondary necrosis.

89 RESULTS

90 **Canonical inflammasomes trigger a rapid secondary necrosis in absence of GSDMD**

91 The canonical and non-canonical inflammasome pathways converge on the caspase-
92 dependent cleavage and activation of the pyroptosis executor GSDMD (Shi et al., 2015;
93 Kayagaki et al., 2015). However, while GSDMD is essential for lytic cell death (pyroptosis) after
94 LPS-induced non-canonical inflammasome activation (**Fig. S1A**), *Gsdmd*-deficiency only
95 delays cell lysis after engagement of canonical inflammasome receptors, such as AIM2 (**Fig.**
96 **1A, S1B-D**), NLRC4 (**Fig. S1B**) and NLRP3 (**Fig. S1B**) (Kayagaki et al., 2015). The absence
97 of caspase-1 and -11 in primary bone marrow derived macrophages (BMDMs), by contrast,
98 showed a much stronger reduction in LDH release and PI influx; and *Asc*-deficiency completely
99 abrogated cell lysis after AIM2 or NLRP3 activation, in line with the reported ASC-dependent
100 activation of apoptosis in absence of caspase-1 (Sagulenko et al., 2013; Pierini et al., 2012;
101 Chen et al., 2015; Man et al., 2013; Vajjhala et al., 2015).

102 We next tested a number of cell death inhibitors for their ability to block cell lysis in *Gsdmd*^{-/-}
103 immortalized BMDMs (iBMDMs) transfected with poly(dA:dT), an activator of the AIM2
104 inflammasome (**Fig. S2**). Neither 7-Cl-O-Nec1 (RIPK1 kinase inhibitor) nor GSK872 (RIPK3
105 kinase inhibitor) were able to delay cell death in *Gsdmd*^{-/-} iBMDMs, thereby excluding a role
106 for necroptosis or complex IIb-dependent apoptosis which require the kinase activity of RIPK3
107 or RIPK1 respectively (Tenev et al., 2011; Feoktistova et al., 2011; He et al., 2009; Zhang et
108 al., 2009; Cho et al., 2009). Similarly, we ruled out the involvement of calpains, calcium-
109 dependent proteases (PD150606, Calpeptin) or cathepsins (pan-cathepsin inhibitor K777),
110 which were previously shown to induce apoptosis through a caspase-3 dependent or
111 independent mechanisms (Chwieralski et al., 2006; Stennicke et al., 1998; Momeni, 2011).
112 Finally, we also tested if caspase inhibitors delayed death in *Gsdmd*^{-/-} or WT iBMDMs.
113 Remarkably, we found that whereas the pan-caspase inhibitor VX765 delayed PI uptake in
114 both WT and *Gsdmd*^{-/-} poly(dA:dT)-transfected cells, the specific caspase-3/-7 inhibitor I only
115 blocked cell death in *Gsdmd*^{-/-} but not in WT cells (**Fig. 1B, Fig. S2**). VX765 failed to prevent
116 cell death in WT cells at later timepoints in accordance with previous studies that showed that
117 pyroptosis is difficult to block pharmaceutically (Schneider et al., 2017).

118 While this suggested that apoptotic executioner caspases were necessary for cell death in
119 *Gsdmd*-deficient cells but dispensable for cell death in WT cells, the speed by which *Gsdmd*-
120 deficient cells underwent apoptosis and subsequently cell lysis was remarkable. *Gsdmd*^{-/-}
121 BMDMs displayed DNA-laddering and processing of caspase-3 to the mature p17 fragment
122 within one hour after poly(dA:dT) transfection, which was faster than even the highest
123 concentrations of either extrinsic or intrinsic apoptosis stimuli tested (**Fig. 1C-D**). It is
124 noteworthy that the highest concentration regularly used to induce apoptosis is yet 20-times

125 lower than the concentration used in our study (Vince et al., 2018). Phenotypically, this rapid
126 activation of caspase-3 resulted in a very fast lytic cell death as measured by PI influx (**Fig.**
127 **1E**) and morphological analysis (**Fig. 1F**). Of note, inflammasome-stimulated *Gsdmd*^{-/-}
128 BMDMs initiated membrane blebbing and apoptotic body formation initially, but rapidly lost this
129 morphology and transitioned into a necrotic state, characterized by extensive membrane
130 ballooning (**Fig. 1F**), similarly to the end-stage of GSDMD-induced pyroptosis (**Fig. S3A-C**).
131 We conclude that inflammasome activation in absence of GSDMD results in rapid cell lysis,
132 which we propose to refer to as 'GSDMD-independent secondary necrosis' to reflect both the
133 rapid transition to the necrotic state and the requirement for the activity of the apoptotic
134 executioner caspases-3/-7.

135

136 **GSDMD-independent secondary necrosis is mainly driven by caspase-3**

137 We next investigated which executioner caspase was required for GSDMD-independent
138 secondary necrosis after caspase-1 activation. High levels of caspase-3/-7 activity was
139 detected in poly(dA:dT)-transfected and *Salmonella*-infected *Gsdmd*^{-/-} and to a lesser degree
140 in *Casp1*^{-/-}/*Casp11*^{-/-} BMDMs, whereas WT or *Asc*^{-/-} BMDMs showed minimal to no activity
141 (**Fig. 2A, Fig. S4A**). Since both caspase-3 and -7 cleave the DEVD peptidic substrate, we next
142 determined which executioner caspase was cleaved in *Gsdmd*^{-/-} cells, but found that both
143 caspase-3 and caspase-7 were rapidly cleaved (**Fig. 2B**). Although, caspase-7 was found in
144 WT and *Gsdmd*-deficient cells, only *Gsdmd*^{-/-} cells display detectable caspase-3/-7 activity
145 and caspase-3 cleavage (**Fig. 2A**). We therefore hypothesized that caspase-3 must account
146 for the DEVDase activity in *Gsdmd*^{-/-} BMDMs.

147 To confirm our hypothesis genetically, we used CRISPR/Cas9 genome engineering to delete
148 either *Casp3* or *Casp7*, or both *Casp-3/7* in *Gsdmd*^{-/-} BMDMs (**Fig. S4B**) and determined the
149 impact of the deletion on GSDMD-independent secondary necrosis after AIM2 inflammasome
150 activation (**Fig. 2C, Fig. S4C**). *Gsdmd*^{-/-}/*Casp3*^{-/-} as well as *Gsdmd*^{-/-}/*Casp3*^{-/-}/*Casp7*^{-/-}
151 iBMDMs were strongly protected against cell death after poly(dA:dT) transfection, while *Casp7*
152 single-deficiency did not provide protection, despite previous reports that caspase-3 and -7
153 function in redundant manner (**Fig. 2C, Fig. S4C**) (Lamkanfi and Kanneganti, 2010; Walsh et
154 al., 2008). Caspase-7 appeared to mainly contribute to the cell death observed in *Gsdmd*^{-/-}
155 /*Casp3*^{-/-} iBMDMs, as these had higher LDH levels than *Gsdmd*^{-/-}/*Casp3*^{-/-}/*Casp7*^{-/-} iBMDMs
156 (**Fig. 2C**). These data were further corroborated by knock-down of caspase-3 or -7 in *Gsdmd*^{-/-}
157 iBMDMs (**Fig. S4D**). Finally, we also examined cell morphology after poly(dA:dT)
158 transfection. *Casp7* knock-out in *Gsdmd*^{-/-} iBMDMs failed to reduce necrotic features and cell
159 lysis, whereas *Gsdmd*^{-/-}/*Casp3*^{-/-} as well as *Gsdmd*^{-/-}/*Casp3*^{-/-}/*Casp7*^{-/-} iBMDMs remained
160 alive and intact (**Fig. 2D**) at 3 hours post treatment. In summary, these results demonstrate

161 that even though both executioner caspases are cleaved during cell death, it is caspase-3 that
162 drives GSDMD-independent secondary necrosis in inflammasome-activated cells.
163 Because caspase-3 was shown to cleave gasdermin-E (GSDME), another member of the
164 gasdermin- family, and was proposed to drive secondary necrosis during prolonged apoptosis,
165 we asked whether lack of GSDMD drives an alternative pathway via caspase-3 mediated
166 GSDME cleavage and pore formation. We thus measured LDH release and PI influx in WT,
167 *Gsdmd*^{-/-}, *Gsdme*^{-/-}, *Gsdmd*^{-/-}/*Gsdme*^{-/-} BMDMs upon activation of the AIM2 inflammasome
168 (**Fig. 2E, S5A**). Surprisingly, although GSDME was cleaved in *Gsdmd*^{-/-} at 1h post poly(dA:dT)
169 transfection, we did not find a contribution of GSDME to cell death in *Gsdmd*^{-/-} BMDMs, since
170 *double* GSDMD/GSDME-*deficiency* did not conferred any additional protection (**Fig. 2E, S5A-**
171 **B**). Furthermore, BMDMs lacking only GSDME were comparable to WT BMDMs, overall
172 suggesting that GSDME does neither contribute to pyroptosis nor GSDMD-independent
173 necrosis.

174

175 **Caspase-1 is required to cause GSDMD-independent secondary necrosis in** 176 **inflammasome-activated cells**

177 Since the ASC speck has been reported to control activation of apoptotic caspases
178 independently of caspase-1 (Sagulenko et al., 2013; Pierini et al., 2012; Schneider et al., 2017;
179 Van Opendenbosch et al., 2017; Lee et al., 2018; Mascarenhas et al., 2017), we next generated
180 *Gsdmd*^{-/-}/*Casp1*^{-/-} BMDMs to determine if caspase-1 was required for GSDMD-independent
181 secondary necrosis (**Fig. 3A**). Deletion of caspase-1 in *Gsdmd*-deficient BMDMs strongly
182 reduced LDH release, caspase-3 processing and caspase-3 activity (**Fig. 3A-C**). LDH levels
183 after 3 and 5 hours of poly(dA:dT) transfection were comparable to *Casp1*^{-/-}/*Casp11*^{-/-}
184 BMDMs, but not as low as in *Asc*^{-/-}, confirming that *Casp1* deletion did not affect the cell death
185 that is caused through the ASC-Caspase-8 axis (**Fig. 3B**). It would theoretically be possible
186 that GSDMD-independent secondary necrosis is not driven by the catalytic activity of caspase-
187 1, but by the formation of a caspase-1-containing scaffold and the assembly of an unknown
188 death inducing complex, in analogy to the scaffolding function of caspase-8 (Henry and Martin,
189 2017). However, we found that poly(dA:dT)-induced PI influx in BMDMs from *Casp1*^{C284A/C284A}
190 mice, which express a catalytically dead caspase-1, was comparable to *Casp1*^{-/-}/*Casp11*^{-/-} or
191 *Casp1*^{-/-} BMDMs, and much lower than PI influx in *Gsdmd*^{-/-}, we formally excluded this
192 possibility (**Fig. 3D**), we formally concluded that caspase-1 enzymatic-activity is required to
193 drive GSDMD-independent secondary necrosis.

194

195 **Bid cleavage is required for mitochondrial damage and GSDMD-independent secondary**
196 **necrosis**

197 While examining the morphology of inflammasome activated BMDMs by confocal microscopy,
198 we found that *Gsdmd*^{-/-} cells were characterized by mitochondrial fragmentation and loss of
199 mitochondrial membrane potential (**Fig. S6A**) and a rapid drop of cellular ATP levels (**Fig. 4A,**
200 **Fig. S6B-D**) as early as 30 min after inflammasome activation. Given this rapid loss of
201 mitochondrial integrity we hypothesized that it was linked to the rapid onset of caspase-3
202 activation and induction of secondary necrosis in *Gsdmd*-deficient cells.

203 An imbalance of pro- and anti-apoptotic Bcl2 family members results in activation of Bax/Bak
204 pore formation and loss of mitochondrial integrity during apoptosis. Often, degradation and/or
205 cleavage of anti-apoptotic Bcl2 proteins as well as activating cleavage of BH3-only protein are
206 responsible for mitochondrial outer membrane permeabilization (MOMP). To identify which
207 pro-apoptotic Bcl2 proteins are processed in *Gsdmd*^{-/-} BMDMs, we made use of Stable Isotope
208 Labeling with Amino acids in Cell culture (SILAC) mass spectrometry approach (Ong et al.,
209 2002). Differentially isotope-labelled immortalized *Gsdmd*^{-/-} and *Asc*^{-/-} BMDMs were
210 transfected with poly(dA:dT), proteins separated by molecular weight using SDS-PAGE, cut
211 according to MW and each slice analyzed by mass spectrometry (Slice-SILAC). The differential
212 analysis of the heavy versus light fraction enabled a comparison between the non-responsive
213 *Asc*^{-/-} and the responsive *Gsdmd*^{-/-}, wherein appearance of smaller fragments in *Gsdmd*^{-/-}
214 indicated potential cleavage. We focused on potential cleavage of Bcl-2 family proteins that
215 indicate their inability to inhibit BH3-only proteins or promote BH3-only proteins to induce
216 mitochondrial outer membrane permeabilization (MOMP) (Bock and Tait, 2019). The anti-
217 apoptotic protein Mcl-1(of Bcl-2, Mcl-1 and Bcl-XL) and the pro-apoptotic proteins Bax, Bak,
218 Bid (but not Bim) were found to be cleaved in *Gsdmd*^{-/-}, but not in *Asc*^{-/-} cells (**Fig. 4B**). Since
219 in type-II cells caspase-8-cleaved tBid translocates to the mitochondria to promote Bax/Bak-
220 dependent pore formation and intrinsic apoptosis, we investigated whether Bid cleavage
221 promoted GSDMD-independent secondary necrosis. Confirming the SILAC data, Bid was
222 found to be rapidly cleaved in *Gsdmd*^{-/-} cells but not in *Asc*^{-/-} after inflammasome activation
223 (**Fig. 4C**). However, since Bid cleavage was also observed in WT and *Casp1*^{-/-}/*Casp11*^{-/-}
224 BMDMs, we proceeded to assess its contribution to GSDMD-independent secondary necrosis
225 genetically by generating *Gsdmd*^{-/-}/*Bid*^{-/-} iBMDMs (**Fig. S7A**). Knocking out *Bid* in *Gsdmd*^{-/-}
226 cells significantly reduced the levels of caspase-3 activity (**Fig. S7B**) after poly(dA:dT)
227 transfection and in agreement with that strongly reduced LDH release and PI uptake were
228 observed (**Fig. 4D, Fig. S7C**). Strikingly, *Gsdmd*^{-/-}/*Bid*^{-/-} cells looked adhered and elongated
229 comparable to untreated iBMDMs upon transfection with poly(dA:dT) which is in contrast to
230 *Gsdmd*^{-/-} iBMDMs which displayed typical necrotic features such as rounding up,
231 permeabilization, shrinkage and blebbing (**Fig. S7D**). In summary, these results show that Bid

232 is an essential mediator of GSDMD-independent secondary necrosis, and suggest that Bid
233 cleavage is required to drive this cell death.

234 **Caspase-1 cleaves Bid to promote caspase-3 activation and cell lysis**

235 Since proteolytic cleavage of Bid precedes MOMP and is required for cell death we next
236 enquired which upstream caspase is responsible for Bid activation. Immunoblotting for the
237 cleaved p18 fragment of caspase-8 suggested that *Gsdmd*^{+/-} BMDMs contain active caspase-
238 8 at 15-30 minutes after poly(dA:dT) transfection, while very little cleaved caspase-8 p18 was
239 found in WT, *Asc*^{-/-} or *Casp1*^{-/-}/*Casp11*^{-/-} BMDMs (**Fig. 5A, S8A**). Interestingly, the relatively
240 low levels of caspase-8 cleavage in *Casp1*^{-/-}/*Casp11*^{-/-} compared to *Gsdmd*^{+/-} BMDMs
241 suggested that direct activation of caspase-8 by the ASC speck was negligible and that instead
242 caspase-8 activation in *Gsdmd*^{+/-} cells depended on the presence caspase-1. However,
243 whether caspase-1 would cleave and activate caspase-8 directly or by an indirect pathway
244 could not be deduced.

245 We next assessed the role of caspase-8 in causing GSDMD-independent secondary necrosis
246 by generating *Gsdmd*^{+/-}/*Casp8*^{-/-} iBMDM lines (**Fig. S8B**). Of note, while *Casp8*-deficiency in
247 mice results in embryonic lethality due to the unchecked activation of RIP3-dependent
248 necroptosis (Oberst et al., 2011; Kaiser et al., 2011), *Casp8*-deficient macrophages were
249 reported to be viable unless stimulated with extrinsic apoptotic triggers (Kang et al., 2004;
250 Cuda et al., 2015; Kaiser et al., 2011). Indeed, when testing if *Gsdmd*^{+/-}/*Casp8*^{-/-} BMDMs
251 showed reduced levels of cell death after induction of apoptosis with the extrinsic apoptosis
252 stimulus TNF α /SMAC we found that cell death was reduced, but not completely abrogated
253 (**Fig. S8C**). The remaining cell death, however, was block when TNF α /SMAC was combined
254 with the RIPK3 kinase inhibitor GSK'872 (**Fig. S8C**). These results confirmed that the cells
255 were indeed *Casp8* knock-outs, and that the necroptotic pathway was only initiated when death
256 receptors were engaged. We next compared LDH release in *Gsdmd*^{+/-} and *Gsdmd*^{+/-}/*Casp8*^{-/-}
257 BMDMs after transfection of the AIM2 inflammasome activator poly(dA:dT). Unexpectedly, we
258 found no difference in LDH release nor PI uptake between these two genotypes (**Fig. 5B,**
259 **S8D**). Furthermore, we were still able to detect Bid cleavage and caspase-3 processing to the
260 active p17 fragment in inflammasome-activated *Gsdmd*^{+/-}/*Casp8*^{-/-} BMDMs (**Fig. 5C-D**).
261 Previous work has implied that Bid can also be a substrate of caspase-1 (Li et al., 1998), since
262 caspase-1 and caspase-8 have partially overlapping substrate spectrum that includes also
263 GSDMD and IL1 β (Orning et al., 2018; Chen et al., 2019; Sarhan et al., 2018; Maelfait et al.,
264 2008). In line with caspase-1 controlling Bid cleavage directly and independently of caspase-
265 8, we found that tBid generation after AIM2 activation was completely abrogated in *Gsdmd*^{+/-}
266 /*Casp1*^{-/-} BMDMs at early timepoint and strongly reduced after prolonged incubation (**Fig. 5E**),
267 and that caspase-1 was able to efficiently convert Bid to tBid in an *in vitro* cleavage assay (**Fig.**

268 **5F**). In summary our data thus far suggest that while Bid cleavage is essential for GSDMD-
269 independent secondary necrosis and high-levels of active caspase-8 are found in these cells,
270 it is caspase-1 and not caspase-8 that processes Bid and induces mitochondrial
271 permeabilization.

272

273 **GSDMD-independent secondary necrosis requires both caspase-8 and caspase-9**

274 Having identified caspase-1, Bid and caspase-3 as the essential drivers of GSDMD-
275 independent secondary necrosis, we next asked if activation of caspase-9 downstream of
276 mitochondrial permeabilization and cytochrome c release provides the link between Bid and
277 caspase-3 activation. We thus generated *Gsdmd^{+/-}/Casp9^{-/-}* iBMDM lines by CRISPR/Cas9
278 genome targeting and verified that they lacked caspase-9 expression and no longer responded
279 to intrinsic apoptosis induction (**Fig. S9A-B**). However, we found that in analogy to *Casp8*-
280 deficiency, knocking out of *Casp9* in *Gsdmd^{+/-}* had only a small impact on poly(dA:dT)-induced
281 secondary necrosis after 5 hours of treatment, while no impact was detectable at earlier
282 timepoint (**Fig. 6A, S9C**). Furthermore, caspase-3 processing was also found to be unaffected
283 in these cell lines (**Fig. 6B**).

284 These results raised the possibility that caspase-8 and caspase-9 activity was redundant or
285 that caspase-1 was driving Bid cleavage and caspase-3 activation somehow independently of
286 both initiator caspases. We addressed these two scenarios by creating *Gsdmd^{+/-}/Casp8^{-/-}*
287 */Casp9^{-/-}* iBMDM lines (**Fig. S9D**) and compared their phenotype after AIM2 inflammasome
288 activation to our other knockout lines. Poly(dA:dT)-transfected *Gsdmd^{+/-}/Casp8^{-/-}/Casp9^{-/-}*
289 BMDMs displayed significantly reduced levels of LDH release compared to *Gsdmd^{+/-}*, *Gsdmd^{-/-}*
290 */Casp8^{-/-}* or *Gsdmd^{+/-}/Casp9^{-/-}* cells (**Fig. 6C**). Consistent with the reduced levels of cell lysis,
291 we also found that caspase-3 processing was significantly reduced in *Gsdmd^{+/-}/Casp8^{-/-}*
292 */Casp9^{-/-}* when compared to the other genotypes (**Fig. 6D**), confirming that activity of either
293 initiator caspase was sufficient to drive caspase-3 activation and GSDMD-independent
294 secondary necrosis.

295

296 **Bid-induced mitochondrial permeabilization is required to release SMAC and promote** 297 **conversion of caspase-3 p19 to p17**

298 The finding that single deficiency in either caspase-8 or caspase-9 had no impact on caspase-
299 3 activation and GSDMD-independent secondary necrosis, while double-deficiency abrogated
300 cell lysis was unexpected and puzzling. Since Bid was essential for GSDMD-independent
301 secondary necrosis while caspase-9 was not, we hypothesized that other factors released from
302 permeabilized mitochondria were required. Besides cytochrome C, which activates Apaf-1 to

303 assemble the apoptosome and promote caspase-9 activity, mitochondria also release ATP
304 and SMAC. SMAC binds IAPs, in particular XIAP, which normally suppresses caspase-3/7 and
305 -9 activity, and thus relieves the block on apoptosis induction (Deveraux et al., 1997; Wu et al.,
306 2000). We thus closely examined caspase-3 processing between poly(dA:dT)-transfected
307 *Gsdmd*^{-/-} and *Gsdmd*^{-/-}/*Bid*^{-/-}, and found that while only the p17 fragment of caspase-3 was
308 found in *Gsdmd*^{-/-} BMDMs, *Gsdmd*^{-/-}/*Bid*^{-/-} featured two cleaved caspase-3 bands, at 19 and
309 17 kDa (**Fig. 6E, S9E**). Previous studies showed that p19 fragment is generated by apical
310 caspases cleaving in the linker domain between the large and small subunit, while the p17 is
311 generated by auto-processing of the pro-peptide by caspase-3 itself (Kavanagh et al., 2014)
312 (**Fig. 6F**). We hypothesised that *Bid*-deficiency delayed IAP release and thus conversion from
313 the p19 to the p17 fragment and full activity of caspase-3 and that this was a critical factor for
314 GSDMD-independent secondary necrosis. Indeed, treatment with the SMAC mimetic AZD
315 5582 increased generation of caspase-3 p17 (**Fig. S9F**), and partially restored cell death in
316 *Gsdmd*^{-/-}/*Bid*^{-/-} BMDMs (**Fig. 6G**). These results suggest that during GSDMD-independent
317 secondary necrosis, Bid cleavage and mitochondrial permeabilization are mainly required for
318 the release of SMAC and subsequent binding to XIAP, but not to drive caspase-9 activation.
319 However, since either caspase-8 or caspase-9 are needed to process caspase-3 (**Fig. 6D**),
320 caspase-1 cannot induce GSDMD-independent secondary necrosis in absence of both initiator
321 caspases (**Fig. 7**).

322

323 DISCUSSION

324 Here we show that the cell lysis that occurs in *Gsdmd*-deficient cells upon activation of
325 canonical inflammasomes is a rapid form of secondary necrosis (referred to as 'GSDMD-
326 independent secondary necrosis' in this manuscript), and that it depends on the caspase-1-
327 dependent activation of either caspase-8 or -9, Bid cleavage, SMAC release and caspase-3
328 activity. Secondary necrosis describes the loss of membrane integrity of apoptotic cells or
329 apoptotic bodies, and is thus appropriate since death in *Gsdmd*-deficient cells relies on initiator
330 caspases as well as the executor caspase-3 and results in a loss of membrane integrity. Yet,
331 it is remarkably different from regular apoptosis in the signaling pathways that underlies its
332 induction, cellular morphology and the speed by which cells undergo death.

333 GSDMD-independent cell lysis is characterized by a rapid loss of mitochondrial potential and
334 rapid activation of caspase-3, and an atypical apoptotic morphology. Indeed, cells undergoing
335 this type of cell death show only initially signs of regular apoptotic blebs or apoptotic body
336 formation, and quickly lose membrane integrity and start ballooning, similarly to pyroptotic
337 cells. This morphology has in the past led to the speculation that caspase-1 might directly or
338 indirectly cleave an alternative lytic cell death executor, such as another gasdermin family
339 member. Indeed, recently Tsuchiya and colleagues proposed that caspase-3 processes
340 GSDME in *Gsdmd*-deficient CL26 cells that harbor dimerizer-activated caspase-1 (Tsuchiya
341 et al., 2019). Our data in primary mouse macrophages however show no involvement of
342 GSDME in GSDMD-independent secondary necrosis (**Fig. 2E, Fig. S5A-B**), even though
343 GSDME is detectable and processed (**Fig. S5B**). This discrepancy is most likely caused by
344 differences in GSDME expression levels between different cell types. Recent results show that
345 a number of cancer cell lines express sufficiently high levels of GSDME to cause pyroptosis
346 upon treatment with apoptosis-inducing chemotherapy drugs (Wang et al., 2017b). It remains
347 to be determined how much GSDME is expressed by CL-26 cells, a murine colorectal
348 carcinoma cell line, compared to macrophages (Tsuchiya et al., 2019), but overwhelming
349 evidence suggest that at least in macrophages, GSDME expression or activity appear to be
350 insufficient to induce GSDME-dependent cell death after caspase-3 activation (Lee et al.,
351 2018; Chen et al., 2019; Sarhan et al., 2018; Vince et al., 2018). Thus, other yet undefined
352 factors drive the lysis of *Gsdmd*-deficient BMDMs.

353 Another striking difference between regular apoptosis and GSDMD-independent secondary
354 necrosis is the signalling pathway underlying caspase-3 activation. Our data show that the
355 main driver of this cell death is active caspase-1, and that it promotes cell death by cleaving
356 several targets. The most critical of these targets appears to be Bid, which is converted by
357 caspase-1 to tBid (independently of caspase-8) and which induces mitochondrial
358 permeabilization and the release of cytochrome C, ATP and SMAC. Moreover, caspase-1 acts

359 as a kind of 'super-initiator' caspase by activating initiator caspases-8/-9. It is worth noting that
360 caspase-8-activation is mostly driven by caspase-1 with a negligible contribution of direct
361 caspase-8 activation at the ASC speck, as evident from much reduced caspase-8 cleavage in
362 *Casp1/Casp11*-deficient compared to *Gsdmd*-deficient cells. This could potentially be driven
363 by direct caspase-1-induced cleavage of caspase-8, or by caspase-1 somehow enhancing
364 ASC-dependent caspase-8 activation. Caspase-9 activation however is downstream of Bid
365 cleavage. The requirement for either caspase-8 and -9 appears to stem from the fact that
366 caspase-1 fails to process caspase-3 efficiently, despite previous reports suggesting that
367 caspase-1 cleaved caspase-3 directly (Taabazuing et al., 2017; Sagulenko et al., 2018).
368 However, caspase-1 is efficient enough to activate Bid to induce SMAC release, to relieve
369 inhibition by IAPs and allows full conversion to caspase-3 p17/p12.

370 Our findings are contradicting a recent report by the Suda lab, which proposed that cell death
371 in *Gsdmd*-deficient cells is solely caused by the Bid-caspase-9-caspase-3 axis (Tsuchiya et
372 al., 2019). The discrepancy is potentially related to cell line-intrinsic differences or to the
373 method used to activate caspase-1. Tsuchiya et al. performed experiments in CL26-cells,
374 which for example lack ASC, and thus lack ASC speck-induced activation of caspase-8
375 (Sagulenko et al., 2013; Vajjhala et al., 2015; Fu et al., 2016; Pierini et al., 2012), while we
376 used immortalized macrophages, which recapitulate the behavior of primary BMDMs.
377 Furthermore, they used a dimerizer-based system to activate caspase-1, which most likely
378 induces higher levels of caspase-1 activity compared to physiological inflammasome triggers,
379 and thus might explain why Tsuchiya and colleagues did not observe a role for caspase-8,
380 which we however find necessary to amplify caspase-1 activity after treatment with established
381 canonical inflammasome triggers. However, both studies agree that Bid cleavage is essential
382 for cell death in *Gsdmd*-deficient cells, and that Bid is cleaved by caspase-1 independent of
383 caspase-8.

384 Recent work has revealed a surprisingly high level of redundancy and crosstalk between the
385 apoptotic, necroptotic and pyroptotic cell death pathways. Interestingly, in many cases these
386 pathways or crosstalk are normally not detectable or only turned on when another pathway is
387 inhibited. For example, deletion of caspase-8 or its autoprocessing sites are known to result
388 in activation of RIP3/MLKL-dependent necroptosis, a pathway that can otherwise not be
389 observed, and catalytic-dead caspase-8 results in activation of necroptosis as well pyroptosis
390 (Kaiser et al., 2011; Kang et al., 2018; Oberst et al., 2011). It is assumed that this redundancy
391 developed as a defense mechanism to guard against pathogen-induced inhibition of apoptosis,
392 and accordingly viral inhibitors of the three major cell death pathways have been identified
393 (Taxman et al., 2010; Nailwal and Chan, 2019; Li and Stollar, 2004), which highlights that
394 necroptosis is not an artifact caused by lack of caspase-8 activity. Similarly, it could be
395 speculated that the ability of caspase-1 to induce rapid secondary necrosis by activating

396 apoptotic caspases might have developed as a safeguard against viruses that inhibit GSDMD.
397 Indeed, recently, the pathogenic enterovirus 71, that is known to trigger the NLRP3-
398 inflammasome (Wang et al., 2017a), was shown to interfere with GSDMD activation. In
399 particular the viral protease 3C was shown to cleave GSDMD at Q193/194, interfering with N-
400 terminal fragment formation, oligomerization and GSDMD pore formation (Wang et al., 2015).
401 Furthermore, GSDMD-independent secondary necrosis appears to contribute to the clearance
402 of bacterial infection, as it could be shown that *Gsdmd*^{-/-} mice are less susceptible to infection
403 with *Francisella novicida* compared to *Casp1*- or *Aim2*-deficient animals (Schneider et al.,
404 2017; Kanneganti et al., 2018b). Along the same lines, *Gsdmd*-deficient mice infected with *B.*
405 *thailandensis* show lower CFUs and lower IL-1 β levels than *Casp1/Casp11*-deficient animals
406 (Wang et al., 2019). Similarly, it was reported that peritoneal IL-1 β levels are higher in
407 *Salmonella typhimurium*-infected *Gsdmd*^{-/-} mice than *Casp1*^{-/-} controls (Monteleone et al.,
408 2018). These studies thus allow the conclusion that GSDMD-independent cell death is also
409 engaged *in vivo* and that it allows partial protection against intracellular bacterial pathogens.
410 Unexpectedly however, GSDMD-independent secondary necrosis does not appear to be
411 important in models of autoinflammatory diseases, since *Gsdmd*-deficiency rescues mice
412 expressing mutant NLRP3 or Pypin, linked to Neonatal Onset Multisystem Inflammatory
413 Disease (NOMID) and Familial Mediterranean Fever (FMF) (Xiao et al., 2018; Kanneganti et
414 al., 2018a).

415 Considering that knock-out of GSDMD showed a big improvement in pro-inflammatory
416 symptoms associated with the autoinflammatory disease NOMID and FMF, and the
417 importance of the canonical inflammasome pathway in sterile inflammatory disease, research
418 has focused on the discovery of GSDMD specific inhibitors. To date several inhibitors have
419 been identified, though off target effects and specificity still need to be evaluated in more detail
420 (Rathkey et al., 2018; Sollberger et al., 2018; Rashidi et al., 2019). Furthermore, it is important
421 to consider that caspase-1 activity is unrestrained by these inhibitors, and that thus caspase-
422 1 might induce cell death and inflammation through the back-up pathway described in our
423 study.

424

425 MATERIAL AND METHODS

426 **Antibodies, chemicals and reagents.** Drugs: VX-765 (MedchemExpress), Caspase-3/7
427 inhibitor I (CAS 220509-74-0, Santa Cruz Biotechnology), Q-VD-Oph (Selleck Chemicals),
428 AZD5582 (Selleck Chemicals), 7-Cl-O-Nec1 (Abcam), GSK872 (Selleck Chemicals), K777
429 (Adipogen), PD 150606 (Tocris), Calpeptin (Selleck Chemicals), ABT-737 (Selleck
430 Chemicals), S63845 (Selleck Chemicals), Nigericin (InvivoGen).

431 Antibodies: GSDMD (Ab209845, Abcam), Casp-1 (Casper1, AG-20B-0042-C100, AdipoGen),
432 Tubulin (Ab40742, Abcam), IL-1 β (AF-401-NA, R & D Systems), Caspase-3 (#9662, Cell
433 Signaling Technology), Caspase-7 (#9492, Cell Signaling Technology), Caspase-8 (#9429 and
434 4927, Cell Signaling Technology), Caspase-9 (#9508 and #9504, Cell Signaling Technology),
435 Bid (#2003, Cell Signaling Technology).

436 **Animal experiments.** All experiments were performed with approval from the veterinary office
437 of the Canton de Vaud and according to the guidelines from the Swiss animal protection law
438 (licence VD3257). C57BL/6J mice were purchased from Janvier Labs (France) and housed at
439 specific pathogen-free facility at the University of Lausanne. Mice lacking *Asc*, *Casp1*,
440 *Casp1/11*, *Gsdmd*, *Gsdme* or expressing mutant *Casp1*^{C284A} have been previously described
441 (Chen et al., 2019; Schneider et al., 2017; Mariathasan et al., 2004; Kayagaki et al., 2011). All
442 mice were either generated (*Gsdmd*^{-/-}, *Gsdme*^{-/-}) or back crossed (other lines) in the C56BL/6J
443 background.

444 **Cell culture and immortalization of macrophages.** Primary mouse macrophages (BMDMs)
445 were differentiated for 6 days and cultured for up to 9 days in DMEM (Gibco) supplemented
446 with 10% FCS (Bioconcept), 20% 3T3 supernatant (MCSF), 10% Hepes (Gibco) and 10% non-
447 essential amino acids (Gibco). Immortalization of macrophages was done as previously
448 described (Broz et al., 2010; Blasi et al., 1985). Immortalized macrophages (iBMDMs) were
449 cultured in DMEM complemented with 10% FCS (Bioconcept), 10% MCSF (3T3 supernatant),
450 10% Hepes (Amimed) and 10% non-essential amino acids (Life Technologies). To passage
451 the BMDM and iBMDMs cells were washed with PBS and left to detach at 4°C for 15 min and
452 scraped using cell scrapers (Sarstedt), spun down at 300 g for 5 min at 4°C and resuspended
453 in the appropriate amount of medium.

454

455 **Crispr genome editing in immortalized macrophages.** *Bid*⁻, *Casp9*⁻, *Casp8*⁻, *Casp*
456 *8/Casp9*⁻, *Casp1*⁻, *Casp3*⁻, *Casp7*⁻ and *Casp3/7*-deficient immortalized BMDM (iBMDM) were
457 generated using the genome editing system Alt-R-CRISPR/Cas (IDT) according to the
458 manufacturer's protocol. Briefly, the gene-specific targeting crRNA (*Bid*:
459 TGGCTGTACTCGCCAAGAGC TGG Caspase-9: CACACGCACGGGCTCCAAC TGG,
460 Caspase-8: CTTCTAGACTGCAACCGAG AGG, Caspase-1:
461 AATGAAGACTGCTACCTGGC AGG, Caspase-7: GATAAG TGGGCACTCGGTCC TGG,
462 Caspase-3: AATGTCATCTCGCTCTGGTA CGG or TGGGCCTGAAATACCAAGTC AGG)
463 was mixed with the universal RNA oligo tracrRNA to form a gRNA complex (crRNA:-
464 tracrRNA). The addition of the recombinant Cas9 nuclease V3 allowed the formation of an
465 RNP complex specific for targeting the desired genes. The tracrRNA only or RNP complexes
466 were subsequently reverse-transfected into either WT or *Gsdmd*^{-/-} immortalized iBMDM using

467 RNAiMax (Invitrogen). The bulk population was tested for successful gene mutation using the
468 T7 endonuclease digestion assay as follows: cells were lysed by the KAPA Biosystems Kit
469 according to the manufacturer's protocol, and genomic DNA flanking the guide RNA (crRNA)
470 binding site was amplified by PCR using gene-specific primers (Bid: fw:
471 CTGGACATTACTGGGGGCAG, rv: CTCGATAGCCCCTTGGTGTC, Caspase-9: fw:
472 CAAGCTCTCCAGACCTGACC, rv: GAGATCTGACGGGCACCATT, Caspase-8: fw:
473 GGGATGTTGGAGGAAGGCAA, rv: GGCACAGACTTTGAGGGGTT, Caspase-1: fw:
474 CAGACAAGATCCTGAGGGCA, rv: AGATGAGGATCCAGCGAGTAT, Caspase-7: fw:
475 TTGCCTGACCCAAG GTTTGT, rv: CCCAGCAACAGGAAAGCAAC; Caspase-3: fw: GTG
476 GGGGATATCGCTGTCAT, rv: TGTGTAAGGATGCGGACTGC). The amplified genomic DNA
477 was used to perform the heteroduplex analysis according to the manufacturer's protocol (IDT).
478 Single clones were derived from the bulk population by limiting dilution, and the absence of
479 protein expression in single clones was verified by immunoblotting and sequencing of genomic
480 regions, where required.

481 **siRNA knockdown.** 2.5×10^5 *Gsdmd*-deficient iBMDMs were seeded per well of a 6-well plate
482 and incubated overnight. For the siRNA transfection, medium was changed to OptiMEM and
483 siRNA transfection was done according to the manufacturer's protocol, transfecting 25 pmol
484 siRNA (non-targeting: siGENOME Non-targeting siRNA Control Pools [D-001206-14,
485 Dharmacon], caspase-3: Casp3 SMART POOL [M-043042-01, Dharmacon], caspase-7:
486 Casp7 SMART POOL [M-057362-01, Dharmacon]) with 7.5 μ l Lipofectamine RNAiMax
487 (Invitrogen) per well. Medium was exchanged for DMEM (10% FCS, 10% MCSF, 1% NeAA,
488 1% HEPES) after 6 hours. 48 hours post transfection cells were collected and reseeded in a
489 96-well plate at 3×10^4 cells/well. Cells were primed and treated as in cell death assays.

490 **Cell death assays.** The cells were seeded in 96-well plates (100ul/well) or 12-well plates (1
491 ml/well) at a density of 0.5×10^6 cells/ml overnight and primed the next day with 100 ng/mL
492 ultrapure LPS-B5 (055:B5, InvivoGen) for 4 hours. AIM2 inflammasome activation was
493 achieved by transfecting 0.4 μ g poly(dA:dT) (InvivoGen) per 10^5 cells. In separate tubes
494 poly(dA:dT) and linear polyethylenimine (Polyscience, 1 μ g per 10^5 cells) were mixed with
495 OptiMEM by vortexing and left for 3 min at room temperature. Then poly(dA:dT) and PEI were
496 mixed together, vortexed shortly and left for 15 min before adding a quarter of the total volume
497 on top of the cells. Transfection was facilitated by spinning cells for 5 min at 300 g at 37°C.
498 *Salmonella enterica* serovar Typhimurium SL1344 and *Francisella tularensis* subsp. *novicida*
499 U112 (*F. novicida*) infection were done in OptiMEM. For *S. Typhimurium* infection bacteria
500 were grown overnight and subcultured 1/40 for 3.5 hours in Luria low salt broth (LB low salt)
501 supplemented with appropriate antibiotics, whereas infection with *Francisella* were done from
502 the overnight culture grown in brain heart infusion (BHI) broth supplemented with 0.2% L-
503 cysteine (Sigma) and appropriate antibiotics. Bacteria were then added on top of the cells in

504 OptiMEM, spun at 300 g for 5 min and incubated at 37°C for the duration of the experiment or
505 extracellular bacterial growth suppressed by addition of gentamycin at 30 min, 120 min post
506 infection for *S. Typhimurium* and *F. novicida* respectively. For the NLRP3 inflammasome
507 activation, LPS-B5 (055:B5, InvivoGen) priming was done in OptiMEM for 4 hours prior to
508 addition of 5 μ M nigericin (Sigma) and incubated for indicated time. Similarly, cells were primed
509 with 100 ng/ml LPS LPS-B5 (055:B5, InvivoGen) for 4 hours in OptiMEM. LPS/FuGeneHD
510 complexes were prepared by mixing 100 μ l Opti-MEM with 2 μ g ultrapure LPS O111:B4
511 (InvivoGen) and 0.5 μ l of FugeneHD (Sigma) per well to be transfected. The transfection
512 mixture was vortexed briefly, incubated for 10 minutes at room temperature and added
513 dropwise to the cells. Plates were centrifuged for 5 minutes at 200 g and 37 °C. Extrinsic
514 apoptosis was induced by adding 100ng/ml TNF- α and the SMAC mimetic AZD5582 at the
515 indicated concentration. Intrinsic apoptosis was induced by addition of the BH3 mimetic small
516 molecule inhibitor ABT-737 in combination with the Mcl-1 inhibitor S63845 at the indicated
517 concentrations.

518 **Cell death and cytokine release measurement.** Cell lysis was assessed by quantifying the
519 amount of lactate dehydrogenase in the cell supernatant using the LDH cytotoxicity kit (Takara)
520 according to the manufacturer's instructions. To measure cell permeabilization, propidium
521 iodide (Thermo Fisher Scientific) was added to the medium at 12.5 μ g/ml and fluorescent
522 emission measured by Cytation5 (Biotek) over time. LDH and PI uptake were normalized to
523 untreated control and 100% lysis. Cytokine release into the supernatant in particular
524 interleukin-1 β was measured by Elisa (ThermoFisher Scientific) according to the
525 manufacturer's instructions.

526 **DNA fragmentation Assay.** DNA fragmentation during apoptosis and pyroptosis was
527 assessed by agarose gel electrophoresis as described before (Kasibhatla et al., 2006). In brief
528 *Gsdmd*^{-/-} BMDMs were seeded in a 12-well plate and treated with apoptotic triggers or
529 transfected with poly(dA:dT) as described under cell death assays.

530 **Cell lysis and immunoblotting.** After treatment of cells, cell supernatant was collected and
531 1x sample buffer (Thermo Fisher) complemented with 66 nM Tris, 2% SDS was added to the
532 cell lysate. The proteins of the supernatant were precipitated on ice using an end
533 concentration of 4% TCA (wt./vol) for 30 min. Supernatant was then spun down at 20 000g for
534 20 min at 4°C washed with 100% Aceton and centrifuged at 20 000 g for 20 min at 4°C. The
535 protein pellet was air-dried and resuspended with the lysate. The samples were boiled for 10
536 min at 70°C and separated by a 10- or 12% SDS page gel. The transfer to the 0.2 μ M PVDF
537 membranes was accomplished by Trans-Blot Turbo system. Membranes were blocked with
538 5% milk in TBS-T and incubates with the primary antibody for 2 hours at RT or overnight.
539 Membranes were washed 3 times with TBS-T and HRP-coupled antibodies added in 5% milk

540 in TBST-T for 1 hour. After washing, membranes were revealed by Fusion imager (VILBER)
541 using Pierce™ ECL Western Blotting Substrate (Thermo Fisher Scientific) or Pierce™ ECL
542 Plus Western Blotting Substrate (Thermo Fisher Scientific).

543 **Live cell imaging.** BMDM or iBMDM were seeded 5×10^4 /well in 8-well tissue culture treated
544 μ -slides (iBidi) or 96-Well Cell Culture Microplates, μ Clear® (Greiner-Bio One) overnight and
545 primed the next day with 100 ng/ml LPS 055:B5 for 4 hours. The AIM2 inflammasome was
546 activated by transfection of poy(dA:dT) (see cell death assay). For time-lapse microscopy cells
547 were incubated with CellTox Green (Promega) 1: 10 000 and AnnexinV (Biolegend) at at
548 500ng/ml or for mitochondrial health assessment MitotrackerGreen and MitotrackerCmXRos
549 were added to OptiMEM at a final concentration of 125 nM. Images were taken every 5 min.
550 or every 15min. respectively. Zeiss LSM800 point scanning confocal microscope equipped
551 with 63x Plan-Apochromat NA 1.4 oil objective, Zeiss ESID detector module, LabTek heating/
552 CO₂ chamber and motorized scanning stage

553 **Slice-SILAC.** *Gsdmd*- and *Asc*-deficient iBMDMs were grown in SILAC DMEM (Thermo
554 Scientific) medium supplemented with 10% dialyzed FBS, 200 mg/ml proline, 150 mg/ml heavy
555 or light lysine and 50 mg/ml arginine respectively. Cells were passaged 5-6 times until 100%
556 labelling was achieved. For the experiment cells were seeded at 5×10^5 /well in 12-well plates
557 overnight and primed the next day with 100 ng/ml LPS 055:B5 for 4h. Poly(dA:dT) transfection
558 was then carried out as described under Cell Death Assays and plates incubated for 3h. Cell
559 were scraped in OptiMEM and proteins precipitated by 4% TCA. The obtained protein pellet
560 was then resuspended in FASP buffer (4% SDS, 0.1 M DTT, 100 mM Tris pH 7.5) heated for
561 5min. at 95°C, sonicated and cleared by 10min. centrifugation at 13 000 rpm. Downstream
562 sample preparation including SDS gel preparation, mass spectrometry as well as data analysis
563 have been described before (Di Micco et al., 2016).

564 **Caspase-activity assay.** Caspase-3/7 activity was either measured by luminescence using
565 the Caspase-Glo® 3/7 (Promega) according to the manufacturer's protocol or by fluorescence.
566 The caspase-activity assay was performed as follows using the fluorescent substrate N-Acetyl-
567 Asp-Glu-Val-Asp-7-amido-4-trifluoromethylcoumarin (Sigma-Aldrich): Cells were lysed cells
568 directly in the medium by adding 5x Lysis buffer (250 mM Hepes, 25 mM CHAPS, 25 mM DTT)
569 and pipetting up and down. 30 μ l of lysed cells was incubated with 30 μ l of 2x Assay buffer (40
570 mM Hepes, 200 mM NaCl, 2mM EDTA, 0.2% CHAPS 20% Sucrose, 20 mM DTT) and 50 μ M
571 final concentration of substrate in black opaque OptiPlate-96 (PerkinElmer) and read at
572 400/505 at 37°C every 2 min. for 10 min.

573 **Metabolic activity – ATP content.** Metabolic activity was measured by TiterGlo (Promega)
574 according to the manufacturer's protocol. In brief cells plus 25 μ l supernatant were incubated

575 with 25 μ l TiterGlo shook for 2min at 600 rpm and incubated for 10 min. at room temperature
576 before reading.

577 **In vitro caspase-cleavage assay.** Active recombinant caspase-1 was purified as described
578 before (Sborgi et al., 2016). For the *in vitro* cleavage Assay cell lysate from *iGsdmd^{-/-}/Casp-*
579 *3^{-/-}/Casp-7^{-/-}* was prepared as described before (Boucher et al., 2012). Briefly, cells were lysed
580 in ice-cold buffer (50 mM Hepes pH 7.4, 150 mM NaCl, 1% Igepal) and incubated on ice for
581 30 min. Cellular proteins were recovered by centrifugation at 7,000 \times g for 10 min and kept at
582 -80 °C in 30 μ L aliquots. Purified active caspase-1 (50 nM, 100 nM) was added to cell lysate
583 and incubated for 2 h at 37°C. The mixture was then analysed by immunoblot.

584

585 ACKNOWLEDGEMENTS

586 This work was supported by grants from the European Research Council (ERC-2017-CoG—
587 770988—InflamCellDeath) to P.B. .W.C is supported by a Marie Skłodowska-Curie Actions
588 (MSCA) incoming fellowship (MSCA-IF-2018-838252. We thank Prof. Dr. Thomas Henry and
589 Prof. Dr. Olaf Gross for sharing *Asc*^{-/-}, *Casp1*^{-/-} and *Casp*^{C284A/C284A} bone marrow respectively,
590 and Vanessa Mack for technical assistance. In addition, we would also like to thank the UNIL
591 microscopy and proteomics core facilities for help with data generation and analysis.

592

593 AUTHORS CONTRIBUTIONS

594 RH designed, performed and analysed all experiments with the exception of the time-lapse
595 microscopy in SFig. 2, *in vitro* cleavage studies and experiments in SFig. 1A, Fig. 6G that were
596 performed by KS, DB, BD, and KWC respectively. MD and DH contributed to the generation
597 of CRISPR knockouts. RH and PB designed the study and wrote the paper.

598

599 CONFLICT OF INTEREST

600 The authors declare no commercial or financial conflict of interest.

601

REFERENCES

- 602 Aglietti, R.A., A. Estevez, A. Gupta, M.G. Ramirez, P.S. Liu, N. Kayagaki, C. Ciferri, V.M.
603 Dixit, and E.C. Dueber. 2016. GsdmD p30 elicited by caspase-11 during pyroptosis
604 forms pores in membranes. *Proc. Natl. Acad. Sci.* 113:7858–63.
605 doi:10.1073/pnas.1607769113.
- 606 Blasi, E., B.J. Mathieson, L. Varesio, J.L. Cleveland, P.A. Borchert, and U.R. Rapp. 1985.
607 Selective immortalization of murine macrophages from fresh bone marrow by a raf/myc
608 recombinant murine retrovirus. *Nature.* 318:667–670. doi:10.1038/318667a0.
- 609 Bock, F.J., and S.W.G. Tait. 2019. Mitochondria as multifaceted regulators of cell death. *Nat.*
610 *Rev. Mol. Cell Biol.* 21:85–100. doi:10.1038/s41580-019-0173-8.
- 611 Boucher, D., V. Blais, and J.-B. Denault. 2012. Caspase-7 uses an exosite to promote
612 poly(ADP ribose) polymerase 1 proteolysis. *Proc. Natl. Acad. Sci.*
613 doi:10.1073/pnas.1200934109.
- 614 Bratton, S.B., J. Lewis, M. Butterworth, C.S. Duckett, and G.M. Cohen. 2002. XIAP inhibition
615 of caspase-3 preserves its association with the Apaf-1 apoptosome and prevents CD95-
616 and Bax-induced apoptosis. *Cell Death Differ.* 9:881–892. doi:10.1038/sj.cdd.4401069.
- 617 Broz, P., and V.M. Dixit. 2016. Inflammasomes: mechanism of assembly, regulation and
618 signalling. *Nat. Rev. Immunol.* 16:407–20. doi:10.1038/nri.2016.58.
- 619 Broz, P., J. Von Moltke, J.W. Jones, R.E. Vance, and D.M. Monack. 2010. Differential
620 requirement for caspase-1 autoproteolysis in pathogen-induced cell death and cytokine
621 processing. *Cell Host Microbe.* 8:471–483. doi:10.1016/j.chom.2010.11.007.
- 622 Chen, K.W., B. Demarco, R. Heilig, K. Shkarina, A. Boettcher, C.J. Farady, P. Pelczar, and
623 P. Broz. 2019. Extrinsic and intrinsic apoptosis activate pannexin-1 to drive NLRP3
624 inflammasome assembly. *EMBO J.* 38:e101638. doi:10.15252/embj.2019101638.
- 625 Chen, M., Y. Xing, A. Lu, W. Fang, B. Sun, C. Chen, W. Liao, and G. Meng. 2015.
626 Internalized *Cryptococcus neoformans* Activates the Canonical Caspase-1 and the
627 Noncanonical Caspase-8 Inflammasomes. *J. Immunol.* 195:4962–4972.
628 doi:10.4049/jimmunol.1500865.
- 629 Cho, Y.S., S. Challa, D. Moquin, R. Genga, T.D. Ray, M. Guildford, and F.K.-M.M. Chan.
630 2009. Phosphorylation-Driven Assembly of the RIP1-RIP3 Complex Regulates
631 Programmed Necrosis and Virus-Induced Inflammation. *Cell.* 137:1112–1123.
632 doi:10.1016/j.cell.2009.05.037.

633 Chwieralski, C.E., T. Welte, and F. Bühling. 2006. Cathepsin-regulated apoptosis. *Apoptosis*.
634 11:143–149. doi:10.1007/s10495-006-3486-y.

635 Cuda, C.M., A. V. Misharin, S. Khare, R. Saber, F.N. Tsai, A.M. Archer, P.J. Homan, G.K.
636 Haines, J. Hutcheson, A. Dorfleutner, G.R.S. Budinger, C. Stehlik, and H. Perlman.
637 2015. Conditional deletion of caspase-8 in macrophages alters macrophage activation
638 in a RIPK-dependent manner. *Arthritis Res. Ther.* 17:1–16. doi:10.1186/s13075-015-
639 0794-z.

640 Deveraux, Q.L., R. Takahashi, G.S. Salvesen, and J.C. Reed. 1997. X-linked IAP is a direct
641 inhibitor of cell-death proteases. *Nature*. 388:300–304. doi:10.1038/40901.

642 Ding, J., K. Wang, W. Liu, Y. She, Q. Sun, J. Shi, H. Sun, D. Wang, and F. Shao. 2016.
643 Pore-forming activity and structural autoinhibition of the gasdermin family. *Nature*.
644 535:111–116. doi:10.1038/nature18590.

645 Du, C., M. Fang, Y. Li, L. Li, and X. Wang. 2000. Smac, a Mitochondrial Protein that
646 Promotes Cytochrome c–Dependent Caspase Activation by Eliminating IAP Inhibition.
647 *Cell*. 102:33–42. doi:10.1016/S0092-8674(00)00008-8.

648 Feoktistova, M., P. Geserick, B. Kellert, D.P. Dimitrova, C. Langlais, M. Hupe, K. Cain, M.
649 MacFarlane, G. Häcker, and M. Leverkus. 2011. CIAPs Block Ripoptosome Formation,
650 a RIP1/Caspase-8 Containing Intracellular Cell Death Complex Differentially Regulated
651 by cFLIP Isoforms. *Mol. Cell*. 43:449–463. doi:10.1016/j.molcel.2011.06.011.

652 Fu, T.M., Y. Li, A. Lu, Z. Li, P.R. Vajjhala, A.C. Cruz, D.B. Srivastava, F. DiMaio, P.A.
653 Penczek, R.M. Siegel, K.J. Stacey, E.H. Egelman, and H. Wu. 2016. Cryo-EM Structure
654 of Caspase-8 Tandem DED Filament Reveals Assembly and Regulation Mechanisms of
655 the Death-Inducing Signaling Complex. *Mol. Cell*. 64:236–250.
656 doi:10.1016/j.molcel.2016.09.009.

657 Hagar, J.A., D.A. Powell, Y. Aachoui, R.K. Ernst, and E.A. Miao. 2013. Cytoplasmic LPS
658 activates caspase-11: Implications in TLR4-independent endotoxic shock. *Science (80-
659).* 341:1250–1253. doi:10.1126/science.1240988.

660 He, S., L. Wang, L. Miao, T. Wang, F. Du, L. Zhao, and X. Wang. 2009. Receptor Interacting
661 Protein Kinase-3 Determines Cellular Necrotic Response to TNF- α . *Cell*. 137:1100–
662 1111. doi:10.1016/j.cell.2009.05.021.

663 He, W., H. Wan, L. Hu, P. Chen, X. Wang, Z. Huang, Z.-H. Yang, C.-Q. Zhong, and J. Han.
664 2015. Gasdermin D is an executor of pyroptosis and required for interleukin-1 β
665 secretion. *Cell Res*. 25:1285–98. doi:10.1038/cr.2015.139.

666 Henry, C.M., and S.J. Martin. 2017. Caspase-8 Acts in a Non-enzymatic Role as a Scaffold
667 for Assembly of a Pro-inflammatory “FADDosome” Complex upon TRAIL Stimulation.
668 *Mol. Cell.* 65:715-729.e5. doi:10.1016/j.molcel.2017.01.022.

669 Jost, P.J., S. Grabow, D. Gray, M.D. McKenzie, U. Nachbur, D.C.S. Huang, P. Bouillet, H.E.
670 Thomas, C. Borner, J. Silke, A. Strasser, and T. Kaufmann. 2009. XIAP discriminates
671 between type I and type II FAS-induced apoptosis. *Nature.* 460:1035–1039.
672 doi:10.1038/nature08229.

673 Kaiser, W.J., J.W. Upton, A.B. Long, D. Livingston-Rosanoff, L.P. Daley-Bauer, R. Hakem, T.
674 Caspary, and E.S. Mocarski. 2011. RIP3 mediates the embryonic lethality of caspase-8-
675 deficient mice. *Nature.* 471:368–373. doi:10.1038/nature09857.

676 Kang, T.-B., T. Ben-Moshe, E.E. Varfolomeev, Y. Pewzner-Jung, N. Yogev, A. Jurewicz, A.
677 Waisman, O. Brenner, R. Haffner, E. Gustafsson, P. Ramakrishnan, T. Lapidot, and D.
678 Wallach. 2004. Caspase-8 Serves Both Apoptotic and Nonapoptotic Roles. *J. Immunol.*
679 173:2976–2984. doi:10.4049/jimmunol.173.5.2976.

680 Kang, T.B., J.S. Jeong, S.H. Yang, A. Kovalenko, and D. Wallach. 2018. Caspase-8
681 deficiency in mouse embryos triggers chronic RIPK1-dependent activation of
682 inflammatory genes, independently of RIPK3. *Cell Death Differ.* 25:1107–1117.
683 doi:10.1038/s41418-018-0104-9.

684 Kanneganti, A., R.K.S. Malireddi, P.H. V Saavedra, L. Vande Walle, H. Van Gorp, H.
685 Kambara, H. Tillman, P. Vogel, H.R. Luo, R.J. Xavier, H. Chi, and M. Lamkanfi. 2018a.
686 GSDMD is critical for autoinflammatory pathology in a mouse model of Familial
687 Mediterranean Fever. *J. Exp. Med.* 215:1519–1529. doi:10.1084/jem.20172060.

688 Kanneganti, T.-D., Q. Zhu, M. Zheng, A. Balakrishnan, and R. Karki. 2018b. Francisella
689 novicida Protection against Activation and Is Required for Host Gasdermin D Promotes
690 AIM2 Inflammasome. doi:10.4049/jimmunol.1800788.

691 Kasibhatla, S., G.P. Amarante-Mendes, D. Finucane, T. Brunner, E. Bossy-Wetzel, and D.R.
692 Green. 2006. Analysis of DNA Fragmentation Using Agarose Gel Electrophoresis. *Cold*
693 *Spring Harb. Protoc.* 2006.pdb.prot4429. doi:10.1101/pdb.prot4429.

694 Kavanagh, E., J. Rodhe, M.A. Burguillos, J.L. Venero, and B. Joseph. 2014. Regulation of
695 caspase-3 processing by cIAP2 controls the switch between pro-inflammatory activation
696 and cell death in microglia. *Cell Death Dis.* 5:e1565–e1565.
697 doi:10.1038/cddis.2014.514.

698 Kayagaki, N., I.B. Stowe, B.L. Lee, K. O’Rourke, K. Anderson, S. Warming, T. Cuellar, B.
699 Haley, M. Roose-Girma, Q.T. Phung, P.S. Liu, J.R. Lill, H. Li, J. Wu, S. Kummerfeld, J.

700 Zhang, W.P. Lee, S.J. Snipas, G.S. Salvesen, L.X. Morris, L. Fitzgerald, Y. Zhang, E.M.
701 Bertram, C.C. Goodnow, and V.M. Dixit. 2015. Caspase-11 cleaves gasdermin D for
702 non-canonical inflammasome signalling. *Nature*. 526:666–671.
703 doi:10.1038/nature15541.

704 Kayagaki, N., S. Warming, M. Lamkanfi, L. Vande Walle, S. Louie, J. Dong, K. Newton, Y.
705 Qu, J. Liu, S. Heldens, J. Zhang, W.P. Lee, M. Roose-Girma, and V.M. Dixit. 2011. Non-
706 canonical inflammasome activation targets caspase-11. *Nature*. 479:117–121.
707 doi:10.1038/nature10558.

708 Kayagaki, N., M.T. Wong, I.B. Stowe, S.R. Ramani, L.C. Gonzalez, S. Akashi-takamura, K.
709 Miyake, J. Zhang, W.P. Lee, L.S. Forsberg, R.W. Carlson, and V.M. Dixit. 2013.
710 Independent of TLR4. *Science (80-.)*. 130:1246–1249. doi:10.5061/dryad.bt51g.

711 Lamkanfi, M., and T.-D. Kanneganti. 2010. Caspase-7: a protease involved in apoptosis and
712 inflammation. *Int. J. Biochem. Cell Biol.* 42:21–4. doi:10.1016/j.biocel.2009.09.013.

713 Lamkanfi, M., T.-D. Kanneganti, P. Van Damme, T. Vanden Berghe, I. Vanoverberghe, J.
714 Vandekerckhove, P. Vandenabeele, K. Gevaert, and G. Núñez. 2008. Targeted
715 peptidecentric proteomics reveals caspase-7 as a substrate of the caspase-1
716 inflammasomes. *Mol. Cell. Proteomics*. 7:2350–63. doi:10.1074/mcp.M800132-
717 MCP200.

718 Lee, B.L., K.M. Mirrashidi, I.B. Stowe, S.K. Kummerfeld, C. Watanabe, B. Haley, T.L. Cuellar,
719 M. Reichelt, and N. Kayagaki. 2018. ASC- and caspase-8-dependent apoptotic pathway
720 diverges from the NLRC4 inflammasome in macrophages. *Sci. Rep.* 8:3788.
721 doi:10.1038/s41598-018-21998-3.

722 Li, H., H. Zhu, C. Xu, and J. Yuan. 1998. Cleavage of BID by Caspase 8 Mediates the
723 Mitochondrial Damage in the Fas Pathway of Apoptosis. *Cell*. 94:491–501.
724 doi:10.1016/S0092-8674(00)81590-1.

725 Li, M.L., and V. Stollar. 2004. Alphaviruses and apoptosis. *Int. Rev. Immunol.* 23:7–24.
726 doi:10.1080/08830180490265529.

727 Liu, X., Z. Zhang, J. Ruan, Y. Pan, V.G. Magupalli, H. Wu, and J. Lieberman. 2016.
728 Inflammasome-activated gasdermin D causes pyroptosis by forming membrane pores.
729 *Nature*. 535:153–158. doi:10.1038/nature18629.

730 Maelfait, J., E. Vercammen, S. Janssens, P. Schotte, M. Haegman, S. Magez, and R.
731 Beyaert. 2008. Stimulation of Toll-like receptor 3 and 4 induces interleukin-1beta
732 maturation by caspase-8. *J. Exp. Med.* 205:1967–73. doi:10.1084/jem.20071632.

733 Man, S.M., P. Toulomousis, L. Hopkins, T.P. Monie, K.A. Fitzgerald, and C.E. Bryant. 2013.
734 Salmonella Infection Induces Recruitment of Caspase-8 to the Inflammasome To
735 Modulate IL-1 β Production . *J. Immunol.* 191:5239–5246.
736 doi:10.4049/jimmunol.1301581.

737 Mariathasan, S., K. Hewton, D.M. Monack, D. Vucic, D.M. French, W.P. Lee, M. Roose-
738 Girma, S. Erickson, and V.M. Dixit. 2004. Differential activation of the inflammasome by
739 caspase-1 adaptors ASC and Ipaf. *Nature.* 430:213–218. doi:10.1038/nature02664.

740 Mascarenhas, D.P.A., D.M. Cerqueira, M.S.F. Pereira, F.V.S. Castanheira, T.D. Fernandes,
741 G.Z. Manin, L.D. Cunha, and D.S. Zamboni. 2017. Inhibition of caspase-1 or gasdermin-
742 D enable caspase-8 activation in the Naip5/NLRC4/ASC inflammasome. *PLOS Pathog.*
743 13:e1006502. doi:10.1371/journal.ppat.1006502.

744 Masters, S.L., A. Simon, I. Aksentijevich, and D.L. Kastner. 2009. Horror Autoinflammaticus :
745 The Molecular Pathophysiology of Autoinflammatory Disease. *Annu. Rev. Immunol.*
746 27:621–668. doi:10.1146/annurev.immunol.25.022106.141627.

747 Di Micco, A., G. Frera, J. Lugin, Y. Jamilloux, E.-T. Hsu, A. Tardivel, A. De Gassart, L.
748 Zaffalon, B. Bujisic, S. Siegert, M. Quadroni, P. Broz, T. Henry, C.A. Hrycyna, and F.
749 Martinon. 2016. AIM2 inflammasome is activated by pharmacological disruption of
750 nuclear envelope integrity. *Proc. Natl. Acad. Sci. U. S. A.* 113:E4671-80.
751 doi:10.1073/pnas.1602419113.

752 Momeni, H.R. 2011. Role of calpain in apoptosis. *Cell J.* 13:65–72.

753 Monteleone, M., A.C. Stanley, K.W. Chen, M.J. Sweet, J.L. Stow, K.S. Correspondence, D.L.
754 Brown, J.S. Bezbradica, J.B. Von Pein, C.L. Holley, D. Boucher, M.R. Shakespear, R.
755 Kapetanovic, V. Rolfes, K. Schroder, M.J. Sweet, J.L. Stow, and K. Schroder. 2018.
756 Interleukin-1 β Maturation Triggers Its Relocation to the Plasma Membrane for
757 Gasdermin-D-Dependent and -Independent Secretion. *Cell Rep.* 24:1425–1433.
758 doi:10.1016/j.celrep.2018.07.027.

759 Nailwal, H., and F.K.M. Chan. 2019. Necroptosis in anti-viral inflammation. *Cell Death Differ.*
760 26:4–13. doi:10.1038/s41418-018-0172-x.

761 Oberst, A., C.P. Dillon, R. Weinlich, L.L. McCormick, P. Fitzgerald, C. Pop, R. Hakem, G.S.
762 Salvesen, and D.R. Green. 2011. Catalytic activity of the caspase-8-FLIP L complex
763 inhibits RIPK3-dependent necrosis. *Nature.* 471:363–368. doi:10.1038/nature09852.

764 Ong, S.E., B. Blagoev, I. Kratchmarova, D.B. Kristensen, H. Steen, A. Pandey, and M. Mann.
765 2002. Stable isotope labeling by amino acids in cell culture, SILAC, as a simple and
766 accurate approach to expression proteomics. *Mol. Cell. Proteomics.* 1:376–386.

767 doi:10.1074/mcp.M200025-MCP200.

768 Van Opdenbosch, N., H. Van Gorp, M. Verdonckt, P.H.V. Saavedra, N.M. de Vasconcelos,
769 A. Gonçalves, L. Vande Walle, D. Demon, M. Matusiak, F. Van Hauwermeiren, J.
770 D'Hont, T. Hochepped, S. Krautwald, T.-D. Kanneganti, M. Lamkanfi, N. Van
771 Opdenbosch, H. Van Gorp, M. Verdonckt, H. V Pedro, V. Walle, D. Demon, M.
772 Matusiak, F. Van Hauwermeiren, D. Hont, T. Hochepped, S. Krautwald, and T.-D.
773 Kanneganti. 2017. Caspase-1 Engagement and TLR-Induced c-FLIP Expression
774 Suppress ASC/Caspase-8-Dependent Apoptosis by Inflammasome Sensors NLRP1b
775 and NLR4. *Cell Rep.* 21:3427–3444. doi:10.1016/J.CELREP.2017.11.088.

776 Orning, P., D. Weng, K. Starheim, D. Ratner, Z. Best, B. Lee, A. Brooks, S. Xia, H. Wu, M.A.
777 Kelliher, S.B. Berger, P.J. Gough, J. Bertin, M.M. Proulx, J.D. Goguen, N. Kayagaki,
778 K.A. Fitzgerald, and E. Lien. 2018. Pathogen blockade of TAK1 triggers caspase-8–
779 dependent cleavage of gasdermin D and cell death. *Science (80-.)*. 2818:eaau2818.
780 doi:10.1126/science.aau2818.

781 Pierini, R., C. Juruj, M. Perret, C.L. Jones, P. Mangeot, D.S. Weiss, and T. Henry. 2012.
782 AIM2/ASC triggers caspase-8-dependent apoptosis in Francisella-infected caspase-1-
783 deficient macrophages. *Cell Death Differ.* 19:1709–1721. doi:10.1038/cdd.2012.51.

784 Rashidi, M., D.S. Simpson, A. Hempel, D. Frank, E. Petrie, A. Vince, R. Feltham, J. Murphy,
785 S.M. Chatfield, G.S. Salvesen, J.M. Murphy, I.P. Wicks, and J.E. Vince. 2019. The
786 Pyroptotic Cell Death Effector Gasdermin D Is Activated by Gout-Associated Uric Acid
787 Crystals but Is Dispensable for Cell Death and IL-1 β Release. *J. Immunol.* 203:736–
788 748. doi:10.4049/jimmunol.1900228.

789 Rathkey, J.K., J. Zhao, Z. Liu, Y. Chen, J. Yang, H.C. Kondolf, B.L. Benson, S.M.
790 Chirieleison, A.Y. Huang, G.R. Dubyak, T.S. Xiao, X. Li, and D.W. Abbott. 2018.
791 Chemical disruption of the pyroptotic pore-forming protein gasdermin D inhibits
792 inflammatory cell death and sepsis. *Sci. Immunol.* 3:eaat2738.
793 doi:10.1126/sciimmunol.aat2738.

794 Roy, N., Q.L. Deveraux, R. Takahashi, G.S. Salvesen, J.C. Reed, M. Robertson, T. Ghayur,
795 W.W. Wong, R. Kamen, and R. Weichselbaum. 1997. The c-IAP-1 and c-IAP-2 proteins
796 are direct inhibitors of specific caspases. *EMBO J.* 16:6914–25.
797 doi:10.1093/emboj/16.23.6914.

798 Sagulenko, V., S.J. Thygesen, D.P. Sester, A. Idris, J.A. Cridland, P.R. Vajjhala, T.L.
799 Roberts, K. Schroder, J.E. Vince, J.M. Hill, J. Silke, and K.J. Stacey. 2013. AIM2 and
800 NLRP3 inflammasomes activate both apoptotic and pyroptotic death pathways via ASC.
801 *Cell Death Differ.* 20:1149–1160. doi:10.1038/cdd.2013.37.

802 Sagulenko, V., N. Vitak, P.R. Vajjhala, J.E. Vince, and K.J. Stacey. 2018. Caspase-1 Is an
803 Apical Caspase Leading to Caspase-3 Cleavage in the AIM2 Inflammasome Response,
804 Independent of Caspase-8. *J. Mol. Biol.* 430:238–247. doi:10.1016/J.JMB.2017.10.028.

805 Sarhan, J., B.C. Liu, H.I. Muendlein, P. Li, R. Nilson, A.Y. Tang, A. Rongvaux, S.C. Bunnell,
806 F. Shao, D.R. Green, and A. Poltorak. 2018. Caspase-8 induces cleavage of gasdermin
807 D to elicit pyroptosis during Yersinia infection [Immunology and Inflammation]. *Proc.*
808 *Natl. Acad. Sci. U. S. A.* doi:10.1073/pnas.1809548115.

809 Sborgi, L., S. Rühl, E. Mulvihill, J. Pipercevic, R. Heilig, H. Stahlberg, C. Farady, D. Müller, P.
810 Broz, and S. Hiller. 2016. GSDMD membrane pore formation constitutes the mechanism
811 of pyroptotic cell death. *EMBO J.* 35:e201694696-13. doi:10.15252/emboj.201694696.

812 Schneider, K.S., C.J. Groß, R.F. Dreier, B.S. Saller, R. Mishra, O. Gorka, R. Heilig, E.
813 Meunier, M.S. Dick, T. Čiković, J. Sodenkamp, G. Médard, R. Naumann, J. Ruland, B.
814 Kuster, P. Broz, and O. Groß. 2017. The Inflammasome Drives GSDMD-Independent
815 Secondary Pyroptosis and IL-1 Release in the Absence of Caspase-1 Protease Activity.
816 *Cell Rep.* 21:3846–3859. doi:10.1016/J.CELREP.2017.12.018.

817 Scott, F.L., J.B. Denault, S.J. Riedl, H. Shin, M. Renatus, and G.S. Salvesen. 2005. XIAP
818 inhibits caspase-3 and -7 using two binding sites: Evolutionary conserved mechanism of
819 IAPs. *EMBO J.* 24:645–655. doi:10.1038/sj.emboj.7600544.

820 Shi, J., Y. Zhao, K. Wang, X. Shi, Y. Wang, H. Huang, Y. Zhuang, T. Cai, F. Wang, and F.
821 Shao. 2015. Cleavage of GSDMD by inflammatory caspases determines pyroptotic cell
822 death. *Nature.* 526:660–665. doi:10.1038/nature15514.

823 Shi, J., Y. Zhao, Y. Wang, W. Gao, J. Ding, P. Li, L. Hu, and F. Shao. 2014. Inflammatory
824 caspases are innate immune receptors for intracellular LPS. *Nature.* 514:187–192.
825 doi:10.1038/nature13683.

826 Sollberger, G., A. Choidas, G.L. Burn, P. Habenberger, R. Di Lucrezia, S. Kordes, S.
827 Menninger, J. Eickhoff, P. Nussbaumer, B. Klebl, R. Krüger, A. Herzig, and A.
828 Zychlinsky. 2018. Gasdermin D plays a vital role in the generation of neutrophil
829 extracellular traps. 3. *Science Immunology.* 6689 pp.

830 Stennicke, H.R., J.M. Jürgensmeier, H. Shin, Q. Deveraux, B.B. Wolf, X. Yang, Q. Zhou, H.
831 Michael Ellerby, L.M. Ellerby, D. Bredesen, D.R. Green, J.C. Reed, C.J. Froelich, and
832 G.S. Salvesen. 1998. Pro-caspase-3 Is a Major Physiologic Target of Caspase-8*.

833 Taabazuing, C.Y., M.C. Okondo, and D.A. Bachovchin. 2017. Pyroptosis and Apoptosis
834 Pathways Engage in Bidirectional Crosstalk in Monocytes and Macrophages. *Cell*
835 *Chem. Biol.* 24:507-514.e4. doi:10.1016/J.CHEMBIOL.2017.03.009.

836 Takahashi, R., Q. Deveraux, I. Tamm, K. Welsh, N. Assa-Munt, G.S. Salvesen, and J.C.
837 Reed. 1998. A single BIR domain of XIAP sufficient for inhibiting caspases. *J. Biol.*
838 *Chem.* 273:7787–90. doi:10.1074/JBC.273.14.7787.

839 Taxman, D.J., M.T.H. Huang, and J.P.Y. Ting. 2010. Inflammasome inhibition as a
840 pathogenic stealth mechanism. *Cell Host Microbe.* 8:7–11.
841 doi:10.1016/j.chom.2010.06.005.

842 Tenev, T., K. Bianchi, M. Darding, M. Broemer, C. Langlais, F. Wallberg, A. Zachariou, J.
843 Lopez, M. MacFarlane, K. Cain, and P. Meier. 2011. The Ripoptosome, a Signaling
844 Platform that Assembles in Response to Genotoxic Stress and Loss of IAPs. *Mol. Cell.*
845 43:432–448. doi:10.1016/J.MOLCEL.2011.06.006.

846 Tsuchiya, K., S. Nakajima, S. Hosojima, D. Thi Nguyen, T. Hattori, T. Manh Le, O. Hori, M.R.
847 Mahib, Y. Yamaguchi, M. Miura, T. Kinoshita, H. Kushiya, M. Sakurai, T. Shiroishi,
848 and T. Suda. 2019. Caspase-1 initiates apoptosis in the absence of gasdermin D. *Nat.*
849 *Commun.* 10:2091. doi:10.1038/s41467-019-09753-2.

850 Vajjhala, P.R., A. Lu, D.L. Brown, S.W. Pang, V. Sagulenko, D.P. Sester, S.O. Cridland, J.M.
851 Hill, K. Schroder, J.L. Stow, H. Wu, and K.J. Stacey. 2015. The Inflammasome Adaptor
852 ASC Induces Pro-caspase-8 Death Effector Domain Filaments. *J. Biol. Chem.*
853 290:29217–30. doi:10.1074/jbc.M115.687731.

854 Verhagen, A.M., P.G. Ekert, M. Pakusch, J. Silke, L.M. Connolly, G.E. Reid, R.L. Moritz, R.J.
855 Simpson, and D.L. Vaux. 2000. Identification of DIABLO, a mammalian protein that
856 promotes apoptosis by binding to and antagonizing IAP proteins. *Cell.* 102:43–53.
857 doi:10.1016/S0092-8674(00)00009-X.

858 Vince, J.E., D. De Nardo, W. Gao, A.J. Vince, C. Hall, K. McArthur, D. Simpson, S. Vijayaraj,
859 L.M. Lindqvist, P. Bouillet, M.A. Rizzacasa, S.M. Man, J. Silke, S.L. Masters, G.
860 Lessene, D.C.S. Huang, D.H.D. Gray, B.T. Kile, F. Shao, and K.E. Lawlor. 2018. The
861 Mitochondrial Apoptotic Effectors BAX/BAK Activate Caspase-3 and -7 to Trigger
862 NLRP3 Inflammasome and Caspase-8 Driven IL-1 β Activation. *Cell Rep.* 25:2339-
863 2353.e4. doi:10.1016/j.celrep.2018.10.103.

864 Walsh, J.G., S.P. Cullen, C. Sheridan, A.U. Lüthi, C. Gerner, and S.J. Martin. 2008.
865 Executioner caspase-3 and caspase-7 are functionally distinct proteases. *Proc. Natl.*
866 *Acad. Sci. U. S. A.* 105:12815–12819. doi:10.1073/pnas.0707715105.

867 Wang, H., X. Lei, X. Xiao, C. Yang, W. Lu, Z. Huang, Q. Leng, Q. Jin, B. He, G. Meng, and J.
868 Wang. 2015. Reciprocal Regulation between Enterovirus 71 and the NLRP3
869 Inflammasome. *Cell Rep.* 12:42–48. doi:10.1016/j.celrep.2015.05.047.

- 870 Wang, J., K. Deobald, and F. Re. 2019. Bacteria through Pyroptosis and Direct Killing of
871 Gasdermin D Protects from Melioidosis. doi:10.4049/jimmunol.1900045.
- 872 Wang, W., F. Xiao, P. Wan, P. Pan, Y. Zhang, F. Liu, K. Wu, Y. Liu, and J. Wu. 2017a. EV71
873 3D Protein Binds with NLRP3 and Enhances the Assembly of Inflammasome Complex.
874 doi:10.1371/journal.ppat.1006123.
- 875 Wang, Y., W. Gao, X. Shi, J. Ding, W. Liu, H. He, K. Wang, and F. Shao. 2017b.
876 Chemotherapy drugs induce pyroptosis through caspase-3 cleavage of a gasdermin.
877 *Nature*. 547:99–103. doi:10.1038/nature22393.
- 878 Wilkinson, J.C., A.S. Wilkinson, F.L. Scott, R.A. Csomos, G.S. Salvesen, and C.S. Duckett.
879 2004. Neutralization of Smac/Diablo by inhibitors of apoptosis (IAPs): A caspase-
880 independent mechanism for apoptotic inhibition. *J. Biol. Chem.* 279:51082–51090.
881 doi:10.1074/jbc.M408655200.
- 882 Wu, G., J. Chai, T.L. Suber, J.W. Wu, C. Du, X. Wang, and Y. Shi. 2000. Structural basis of
883 IAP recognition by Smac/DIABLO. *Nature*. 408:1008–1012. doi:10.1038/35050012.
- 884 Xiao, J., C. Wang, J.-C. Yao, Y. Alippe, C. Xu, D. Kress, R. Civitelli, Y. Abu-Amer, T.-D.
885 Kanneganti, D.C. Link, and G. Mbalaviele. 2018. Gasdermin D mediates the
886 pathogenesis of neonatal-onset multisystem inflammatory disease in mice. *PLOS Biol.*
887 16:e3000047. doi:10.1371/journal.pbio.3000047.
- 888 Zhang, D.-W., J. Shao, J. Lin, N. Zhang, B.-J. Lu, S.-C. Lin, M.-Q. Dong, and J. Han. 2009.
889 RIP3, an Energy Metabolism Regulator That Switches TNF-Induced Cell Death from
890 Apoptosis to Necrosis. *Science (80-.).* 2.

FIGURE LEGENDS

892 **Figure 1. Canonical inflammasome activation *Gsdmd*-deficient macrophages results in**
893 **rapid secondary necrosis.**

894 **(A-B).** LDH release, PI influx and IL-1 β release from LPS-primed WT, *Asc*^{-/-}, *Casp1*^{-/-}/*Casp11*^{-/-}
895 ^{-/-} and *Gsdmd*^{-/-} primary or immortalized bone marrow derived macrophages (BMDMs,
896 iBMDMs) after transfection of poly(dA:dT) in absence or presence of the indicated inhibitors.
897 **(C-E)** DNA cleavage, PI influx and immunoblots showing caspase-3/-7 processing from LPS-
898 primed *Gsdmd*^{-/-} BMDMs transfected with poly(dA:dT) or treated with 100 ng/ml TNF- α plus
899 10, 5 or 1 μ M AZD5582 (extrinsic apoptosis) or 1 μ M ABT-737 plus 10, 1 or 0.5 μ M S63845
900 (intrinsic apoptosis). **(F)** Confocal images of LPS-primed *Gsdmd*^{-/-} BMDMs transfected with
901 poly(dA:dT) or left untreated and stained with CellToxGreen (green). Scalebar 10 μ M. Graphs
902 show mean \pm SD. Data and blot are representative of at least three independent experiments.

903 **Figure 2. Caspase-3 drives GSDMD-independent secondary necrosis in inflammasome**
904 **activated cells**

905 **(A-B).** LDH release, caspase-3/-7 activity (DEVDase activity) and immunoblots showing
906 caspase-3/-7 processing from LPS-primed WT, *Asc*^{-/-}, *Casp1*^{-/-}/*Casp11*^{-/-} and *Gsdmd*^{-/-}
907 primary BMDMs after transfection of poly(dA:dT). **(C)** LDH release from LPS-primed WT, *Asc*^{-/-}
908 ^{-/-}, *Casp1*^{-/-}/*Casp11*^{-/-}, *Gsdmd*^{-/-}, *Gsdmd*^{-/-}/*Casp3*^{-/-}, *Gsdmd*^{-/-}/*Casp7*^{-/-} and *Gsdmd*^{-/-}/*Casp3*^{-/-}/*Casp7*^{-/-}
909 iBMDMs after transfection of poly(dA:dT). **(D)** Confocal images of cells from C.
910 Insets show membrane ballooning in dying cells at 3h post transfection. Scalebar 10 μ m. **(E)**
911 Quantification of LDH release in LPS primed WT, *Asc*^{-/-}, *Casp1*^{-/-}/*Casp11*^{-/-}, *Gsdmd*^{-/-},
912 *Gsdme*^{-/-}, *Gsdmd*^{-/-}/*Gsdme*^{-/-} BMDMs transfected with poly(dA:dT) for 4 hours. Graphs show
913 mean \pm SD. **p \leq 0.01, ***p \leq 0.001, "ns" = no significance (Unpaired t-test). Data and blot are
914 representative of at least three independent experiments.

915 **Figure 3: Caspase-1 is required for GSDMD-independent secondary necrosis**

916 **(A-C).** Immunoblot showing Caspase-1 expression and caspase-3 processing, LDH release
917 and caspase-3/-7 activity (DEVDase activity) from LPS-primed *Gsdmd*^{-/-} and *Gsdmd*^{-/-}
918 ^{-/-}/*Casp1*^{-/-} immortalized BMDMs after transfection of poly(dA:dT). **(D)** PI influx of WT, *Asc*^{-/-},
919 *Casp1*^{-/-}/*Casp11*^{-/-}, *Casp1*^{-/-}, *Casp1*^{C284A/C284A} and *Gsdmd*^{-/-} primary BMDMs after
920 transfection of poly(dA:dT). Graphs show mean \pm SD. **p \leq 0.01, ***p \leq 0.001, ****p \leq 0.0001
921 (Unpaired t-test). Data and blot are representative of at least three independent experiments.

922 **Figure 4: Mitochondrial damage is caused by truncated Bid**

923 **(A)** LDH release and TiterGlo measurements from LPS-primed WT, *Asc*^{-/-}, *Casp1*^{-/-}/*Casp11*^{-/-}
924 ^{-/-} and *Gsdmd*^{-/-} primary BMDMs after transfection with poly(dA:dT). **(B)** Schematic cleavage

925 profile of Bcl-2 family members generated from slice SILAC data. Bubble diameters are
926 proportional to the number of quantified peptide matches, whereas the gradient color
927 represents the H/L ratio, as indicated below. The green bubbles (negative log₂H/L) represent
928 protein isoforms reduced in *Gsdmd*^{-/-} iBMDMs compared to *Asc*^{-/-} iBMDMs at 3 hours post
929 poly(dA:dT) transfection; the red bubbles (positive log₂H/L) represent protein isoforms
930 enriched in *Gsdmd*^{-/-} iBMDMs compared to *Asc*^{-/-} iBMDMs. **(C)** Immunoblots showing Bid
931 processing from LPS-primed WT, *Asc*^{-/-}, *Casp1*^{-/-}/*Casp11*^{-/-} and *Gsdmd*^{-/-} primary BMDMs
932 after transfection with poly(dA:dT). **(D)** LDH release from WT, *Asc*^{-/-}, *Casp1*^{-/-}/*Casp11*^{-/-},
933 *Gsdmd*^{-/-} and *Gsdmd*^{-/-}/*Bid*^{-/-} iBMDMs after transfection with poly(dA:dT). Graphs show mean
934 ± SD. *p ≤ 0.05, **p ≤ 0.01, ****p ≤ 0.0001, “ns” = no significance (Unpaired t-test). Data and
935 blots are representative of at least three independent experiments.

936 **Figure 5: Caspase-1 drives Bid processing during GSDMD-independent secondary**
937 **necrosis**

938 **(A)** Immunoblots showing caspase-1, -7, -3, -8 and -9 processing in WT, *Asc*^{-/-}, *Casp1*^{-/-}
939 */Casp11*^{-/-} and *Gsdmd*^{-/-} primary BMDMs after transfection with poly(dA:dT). **(B)** LDH release
940 from WT, *Asc*^{-/-}, *Casp1*^{-/-}/*Casp11*^{-/-}, *Gsdmd*^{-/-} and *Gsdmd*^{-/-} */Casp8*^{-/-} iBMDMs after
941 transfection with poly(dA:dT). **(C)** Immunoblots showing caspase-3 processing in *Gsdmd*^{-/-}
942 and *Gsdmd*^{-/-} */Casp8*^{-/-} iBMDMs after transfection with poly(dA:dT). **(D)** Immunoblots showing
943 Bid cleavage in *Gsdmd*^{-/-} and *Gsdmd*^{-/-} */Casp8*^{-/-} iBMDMs after transfection with poly(dA:dT).
944 **(E)** Immunoblots showing Bid cleavage in *Gsdmd*^{-/-} and *Gsdmd*^{-/-} */Casp1*^{-/-} iBMDMs after
945 transfection with poly(dA:dT). **(F)** *In vitro* cleavage assay showing processing of recombinant
946 Bid by recombinant caspase-1. Graphs show mean ± SD. * “ns” = no significance (Unpaired t-
947 test). Data and blot are representative of at least three independent experiments.

948 **Figure 6: SMAC release and initiator caspases-8/9 are required for GSDMD-**
949 **independent secondary necrosis**

950 **(A)** LDH release from WT, *Asc*^{-/-}, *Casp1*^{-/-}/*Casp11*^{-/-}, *Gsdmd*^{-/-} and *Gsdmd*^{-/-} */Casp9*^{-/-}
951 iBMDMs after transfection with poly(dA:dT). **(B)** Immunoblots showing caspase-3 cleavage in
952 *Gsdmd*^{-/-} and *Gsdmd*^{-/-} */Casp9*^{-/-} iBMDMs after transfection with poly(dA:dT). **(C)** LDH release
953 from WT, *Asc*^{-/-}, *Casp1*^{-/-}/*Casp11*^{-/-}, *Gsdmd*^{-/-}, *Gsdmd*^{-/-} */Casp8*^{-/-}, *Gsdmd*^{-/-} */Casp9*^{-/-} and
954 *Gsdmd*^{-/-} */Casp8*^{-/-} */Casp9*^{-/-} iBMDMs after transfection with poly(dA:dT). **(D)** Immunoblots
955 showing caspase-3 cleavage in *Gsdmd*^{-/-}, *Gsdmd*^{-/-} */Casp8*^{-/-}, *Gsdmd*^{-/-} */Casp9*^{-/-} and *Gsdmd*^{-/-}
956 */Casp8*^{-/-} */Casp9*^{-/-} iBMDMs after transfection with poly(dA:dT). **(E)** Immunoblots showing
957 caspase-3 processing from *Gsdmd*^{-/-} and *Gsdmd*^{-/-} */Bid*^{-/-} iBMDMs after transfection with
958 poly(dA:dT). **(F)** Schematic summary of the mechanism of caspase-3 cleavage and activation.
959 **(G)** PI influx in untreated or poly(dA:dT)-transfected *Gsdmd*^{-/-} */Bid*^{-/-} iBMDMs in presence or

960 absence of the SMAC mimetic AZD5582. Graphs show mean \pm SD. * $p \leq 0.05$, ** $p \leq 0.01$,
961 (Unpaired t-test). Data and blot are representative of at least three independent experiments.

962 **Figure 7: Model of cell death in *Gsdmd*-deficient myeloid cells after activation of**
963 **caspace-1**

964 Model depicting the mechanism of canonical inflammasome activation in WT cells undergoing
965 caspase-1- and GSDMD-dependent pyroptosis and *Gsdmd*^{-/-} cells undergoing caspase-1-
966 induced GSDMD-independent secondary necrosis.

SUPPLEMENTARY FIGURE LEGENDS

967 **Figure S1:**

968 **(A-B)** LDH release from LPS-primed WT, *Asc*^{-/-}, *Casp1*^{-/-}/*Casp11*^{-/-} and *Gsdmd*^{-/-} iBMDMs
969 after transfection of LPS **(A)** or infection with log-phase *S. Typhimurium*, treatment with
970 Nigericin, infection with *F. novicida* or **(B)**. **(C)** PI influx from mock or poly(dA:dT) transfected
971 LPS-primed *Gsdmd*^{-/-} iBMDMs and LDH release from mock or poly(dA:dT) transfected LPS-
972 primed WT, *Asc*^{-/-}, *Casp1*^{-/-}/*Casp11*^{-/-} and *Gsdmd*^{-/-} iBMDMs. **(D)** Immunoblots showing IL-
973 1 β , caspase-1 and GSDMD processing in WT, *Asc*^{-/-}, *Casp1*^{-/-}/*Casp11*^{-/-} and *Gsdmd*^{-/-}
974 BMDMs after transfection of poly(dA:dT). Data and blot are representative of at least three
975 independent experiments.

976 **Figure S2:**

977 PI influx from poly(dA:dT) transfected LPS-primed *Gsdmd*^{-/-} iBMDMs in the presence or
978 absence of the indicated inhibitors added to the cells 30 min. prior and during the experiment
979 at the following concentrations: 50, 25, 12.5, 6.25 μ M VX765, 100, 50, 25, 12.5 μ M Caspase-
980 3/7 specific inhibitor I, 30, 15, 7.5, 3.25 μ M K777, 100, 50, 25, 12.5 μ M, PD150606 and, 100,
981 50, 25, 12.5 μ M Calpeptin, 60, 30, 15, 7.5 μ M 7-Cl-O-Nec1, 100, 50, 25, 12.5 μ M GSK872.
982 Data and blot are representative of at least three independent experiments.

983 **Figure S3:**

984 **(A-B)**. Confocal microscopy images of poly(dA:dT) **(A)** or mock transfected **(B)** WT, *Asc*^{-/-},
985 *Casp1*^{-/-}/*Casp11*^{-/-} and *Gsdmd*^{-/-} primary BMDMs. Cells were stained with CellToxGreen
986 (green) and AnnexinV (red). **(C)** shows selected cells from **(A)**. Scalebar 10 μ m.

987 **Figure S4:**

988 **(A)** LDH release and caspase-3/-7 activity (DEVDase activity) from LPS-primed WT, *Asc*^{-/-},
989 *Casp1*^{-/-}/*Casp11*^{-/-} and *Gsdmd*^{-/-} primary BMDMs after transfection of *Salmonella*

990 Typhimurium at MOI 10. **(B)** Immunoblots for caspase-3 and -7 expression in lysates of
991 *Gsdmd*^{-/-}, *Gsdmd*^{-/-}/*Casp3*^{-/-}, *Gsdmd*^{-/-}/*Casp7*^{-/-} and *Gsdmd*^{-/-}/*Casp3*^{-/-}/*Casp7*^{-/-} iBMDMs.
992 **(C)** PI influx from LPS-primed WT, *Asc*^{-/-}, *Casp1*^{-/-}/*Casp11*^{-/-}, *Gsdmd*^{-/-}, pool of *Gsdmd*^{-/-}
993 /*Casp3*^{-/-} clones (n=3), pool of *Gsdmd*^{-/-}/*Casp7*^{-/-} clones (n=5) and *Gsdmd*^{-/-}/*Casp3*^{-/-}/*Casp7*
994 ^{-/-} iBMDMs after transfection of poly(dA:dT). **(D)** Immunoblots showing caspase-3 and -7
995 expression and LDH release after transfection poly(dA:dT) transfection from LPS-primed
996 *Gsdmd*^{-/-} iBMDMs transfected with control siRNA or siRNA targeting caspase-3, -7 or both.
997 Graphs show mean ± SD. **p ≤ 0.01, ***p ≤ 0.001, (Unpaired t-test). Data and blot are
998 representative of at least three independent experiments.

999 **Figure S5:**

1000 **(A)** Quantification of PI uptake in LPS primed WT, *Asc*^{-/-}, *Casp-1*^{-/-}/*Casp-11*^{-/-}, *Gsdmd*^{-/-},
1001 *Gsdme*^{-/-}, *Gsdmd*^{-/-}/*Gsdme*^{-/-} BMDMs transfected with poly(dA:dT) for 4 hours. **(B)**
1002 Immunoblot for GSDMD, GSDME, caspase-1 and tubulin on pooled supernatant and lysate
1003 samples collected at indicated times. Graph shows mean ± SD. Graph and blot are
1004 representative of at least three independent experiments.

1005 **Figure S6:**

1006 **(A)** Confocal microscopy images showing Mitotracker Green (Green) and Mitotracker Red
1007 (Red) and DIC, 30 min. and 60 min. post poly(dA:dT) transfection into LPS-primed *Gsdmd*^{-/-}
1008 and *Asc*^{-/-} iBMDMs. **(B-D)** LDH release and TiterGlo measurements at 0, 15, 30 and 45 min
1009 or as indicated from LPS-primed WT, *Asc*^{-/-}, *Casp1*^{-/-}/*Casp11*^{-/-} and *Gsdmd*^{-/-} primary
1010 BMDMs after transfection with poly(dA:dT) **(C)** or infection with log-phase *S. Typhimurium* at
1011 MOI 10 **(B,D)**. Scalebar 10 μm. Graphs show mean ± SD. Data and blot are representative of
1012 at least three independent experiments.

1013 **Figure S7:**

1014 **(A)** Immunoblots showing Bid expression in *Gsdmd*^{-/-} and *Gsdmd*^{-/-}/*Bid*^{-/-} iBMDMs. **(B-C)**.
1015 Caspase-3/-7 activity (DEVDase activity) and PI influx in *Gsdmd*^{-/-} and pool of *Gsdmd*^{-/-}/*Bid*^{-/-}
1016 ^{-/-} clones (n=5) iBMDMs after transfection with poly(dA:dT). **(D)** Confocal images of cells of
1017 *Gsdmd*^{-/-} and *Gsdmd*^{-/-}/*Bid*^{-/-} iBMDMs after transfection with poly(dA:dT) for 3 h. Insets show
1018 membrane ballooning in dying cells. Scalebar 10 μm. Graphs show mean ± SD. Data and blot
1019 are representative of at least three independent experiments.

1020 **Figure S8:**

1021 **(A)** Immunoblots showing caspase-1, -7-, -3, -8 and -9 processing in WT, *Asc*^{-/-}, *Casp1*^{-/-}
1022 /*Casp11*^{-/-} and *Gsdmd*^{-/-} primary BMDMs after transfection with poly(dA:dT). **(B)** Immunoblots
1023 showing caspase-8 expression in *Gsdmd*^{-/-} and *Gsdmd*^{-/-}/*Casp8*^{-/-} iBMDMs. **(C)** LDH release

1024 in LPS-primed *Gsdmd*^{-/-} and *Gsdmd*^{-/-}/*Casp8*^{-/-} iBMDMs after transfection with poly(dA:dT)
1025 in the presence of 100 ng/ml TNF- α , the SMAC mimetic AZD5582 (5 μ M) or
1026 AZD5582/GSK872. **(D)** PI influx in *Gsdmd*^{-/-} and pool of *Gsdmd*^{-/-}/*Casp8*^{-/-} clones (n=3)
1027 iBMDMs after transfection with poly(dA:dT). Graphs show mean \pm SD. Data and blot are
1028 representative of at least three independent experiments.

1029 **Figure S9:**

1030 **(A)** Immunoblots showing Casp-9 expression in *Gsdmd*^{-/-} and *Gsdmd*^{-/-}/*Casp9*^{-/-} iBMDMs.
1031 **(B)** PI uptake of *Gsdmd*^{-/-} and *Gsdmd*^{-/-}/*Casp9*^{-/-} iBMDMs treated with 2 μ M ABT737 and 2
1032 μ M S63845. **(C)** PI uptake in LPS-primed and poly(dA:dT)-transfected *Gsdmd*^{-/-} and pool of
1033 *Gsdmd*^{-/-}/*Casp9*^{-/-} clones (n=2) iBMDMs. **(D)** Immunoblots showing Casp-8 and Casp-9
1034 expression in *Gsdmd*^{-/-} and *Gsdmd*^{-/-}/*Casp8*^{-/-}/*Casp9*^{-/-} iBMDMs. **(E)** Immunoblots showing
1035 caspase-3 processing in *Gsdmd*^{-/-} and *Gsdmd*^{-/-}/*Bid*^{-/-} iBMDMs after transfection with
1036 poly(dA:dT). **(F)** Immunoblots showing caspase-3 processing in *Gsdmd*^{-/-} and *Gsdmd*^{-/-}/*Bid*^{-/-}
1037 ^{-/-} iBMDMs after transfection with poly(dA:dT) and treatment with AZD5582. Graphs show mean
1038 \pm SD. Data and blot are representative of at least three independent experiments.

Figure 1

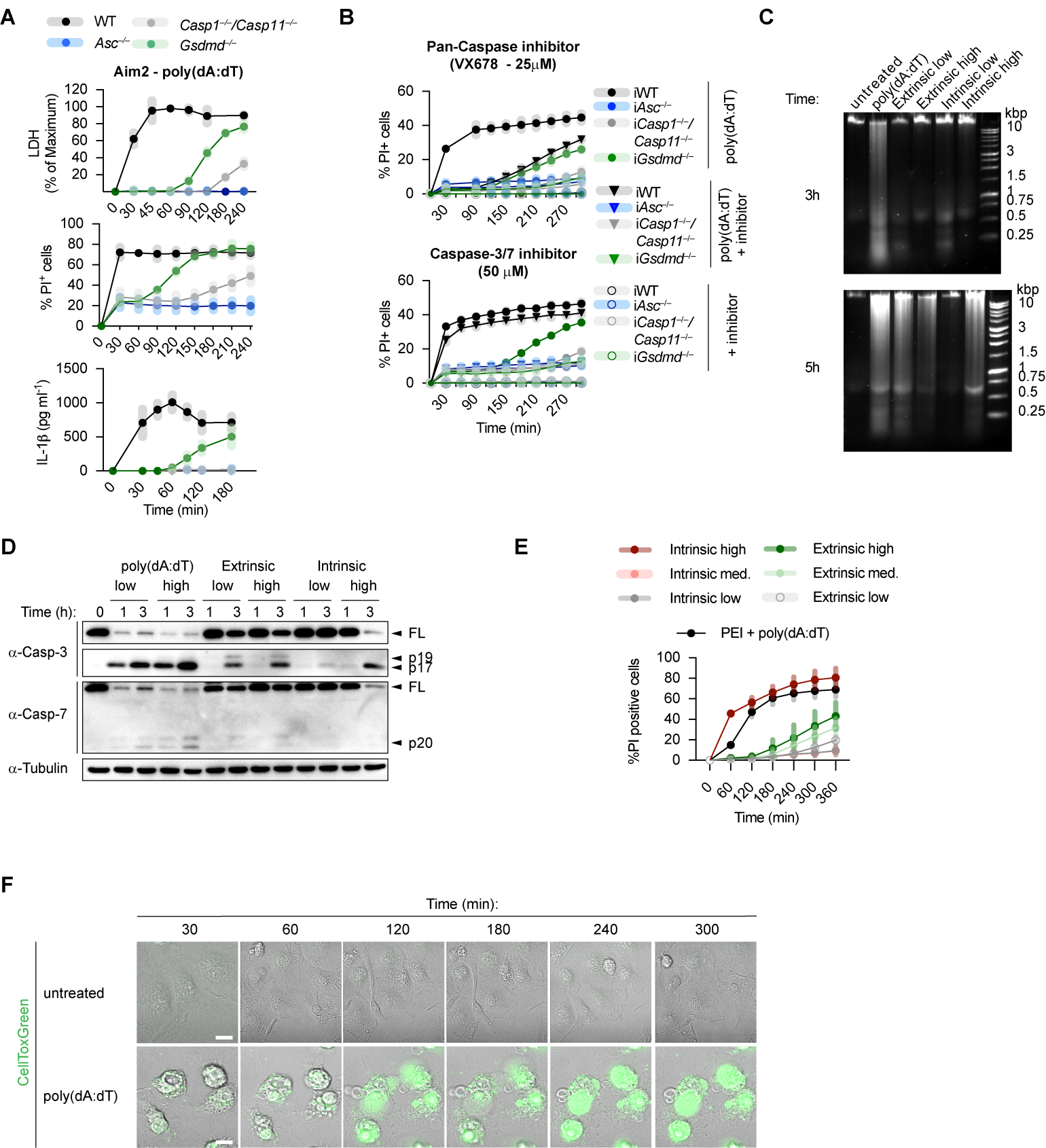


Figure 2

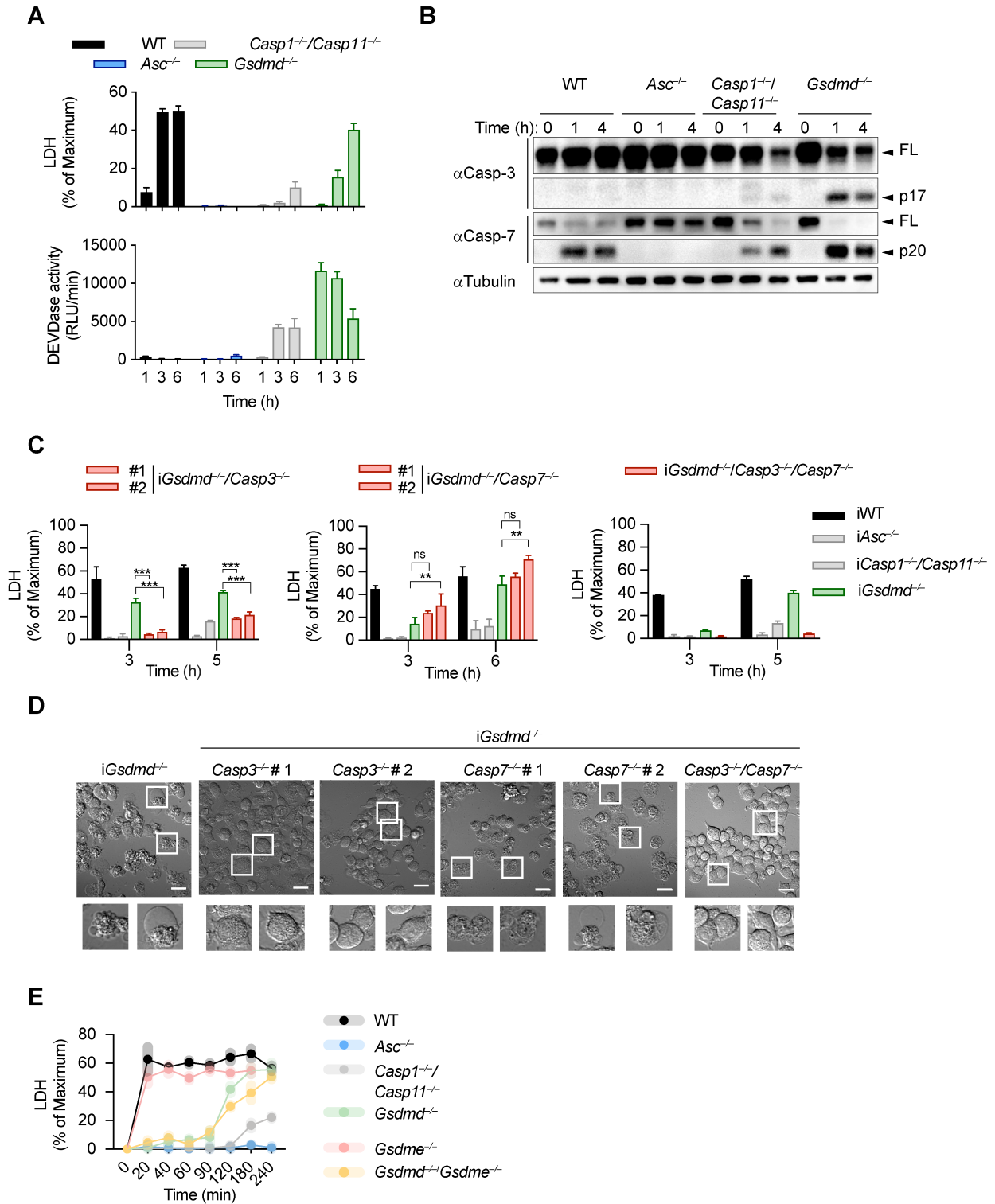
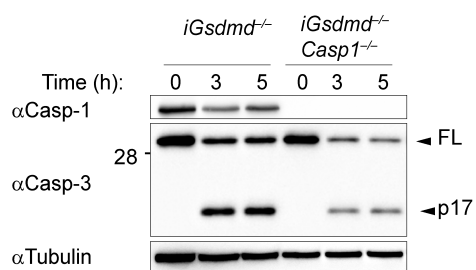
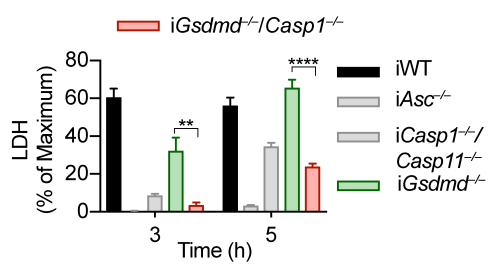


Figure 3

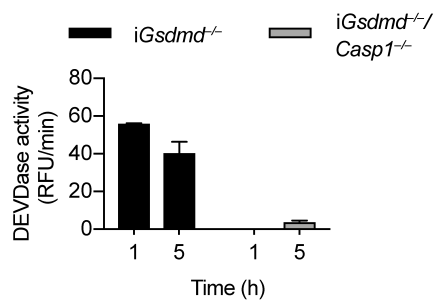
A



B



C



D

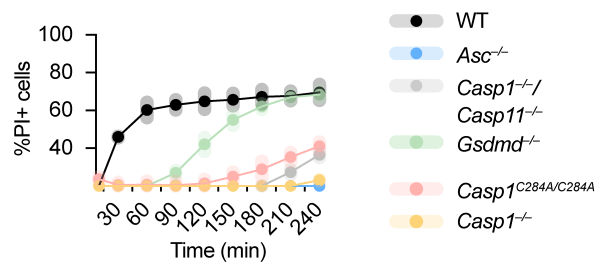
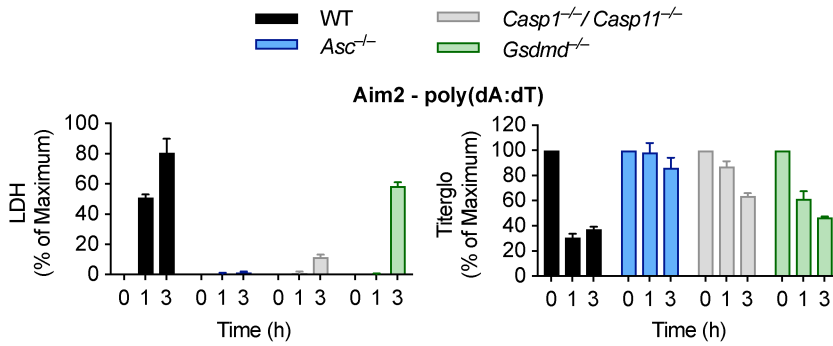
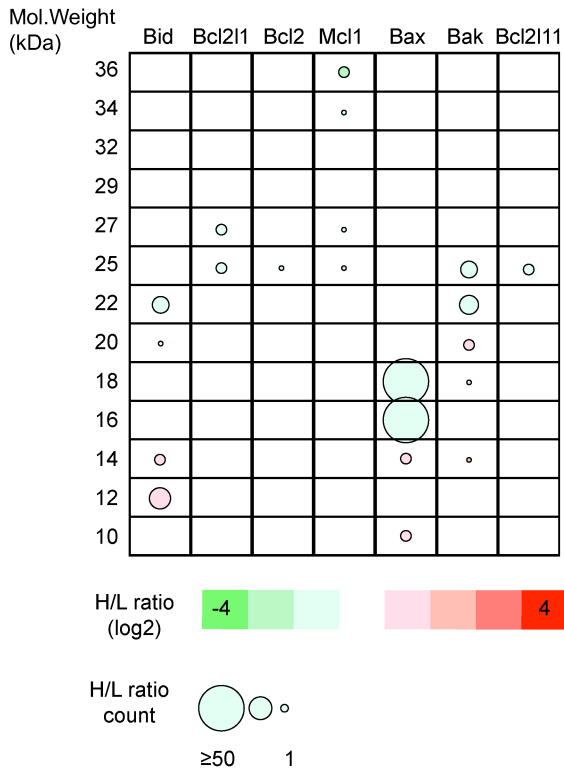


Figure 4

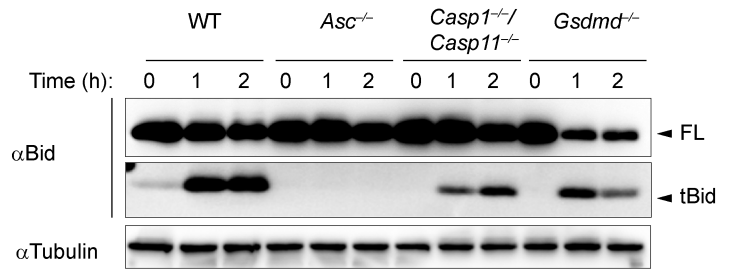
A



B



C



D

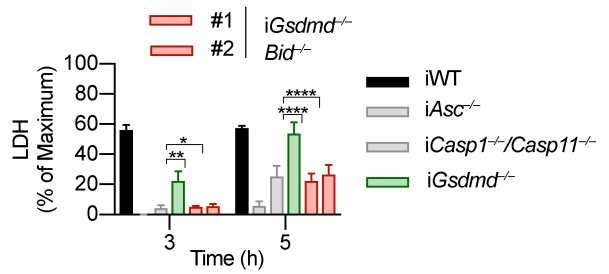


Figure 5

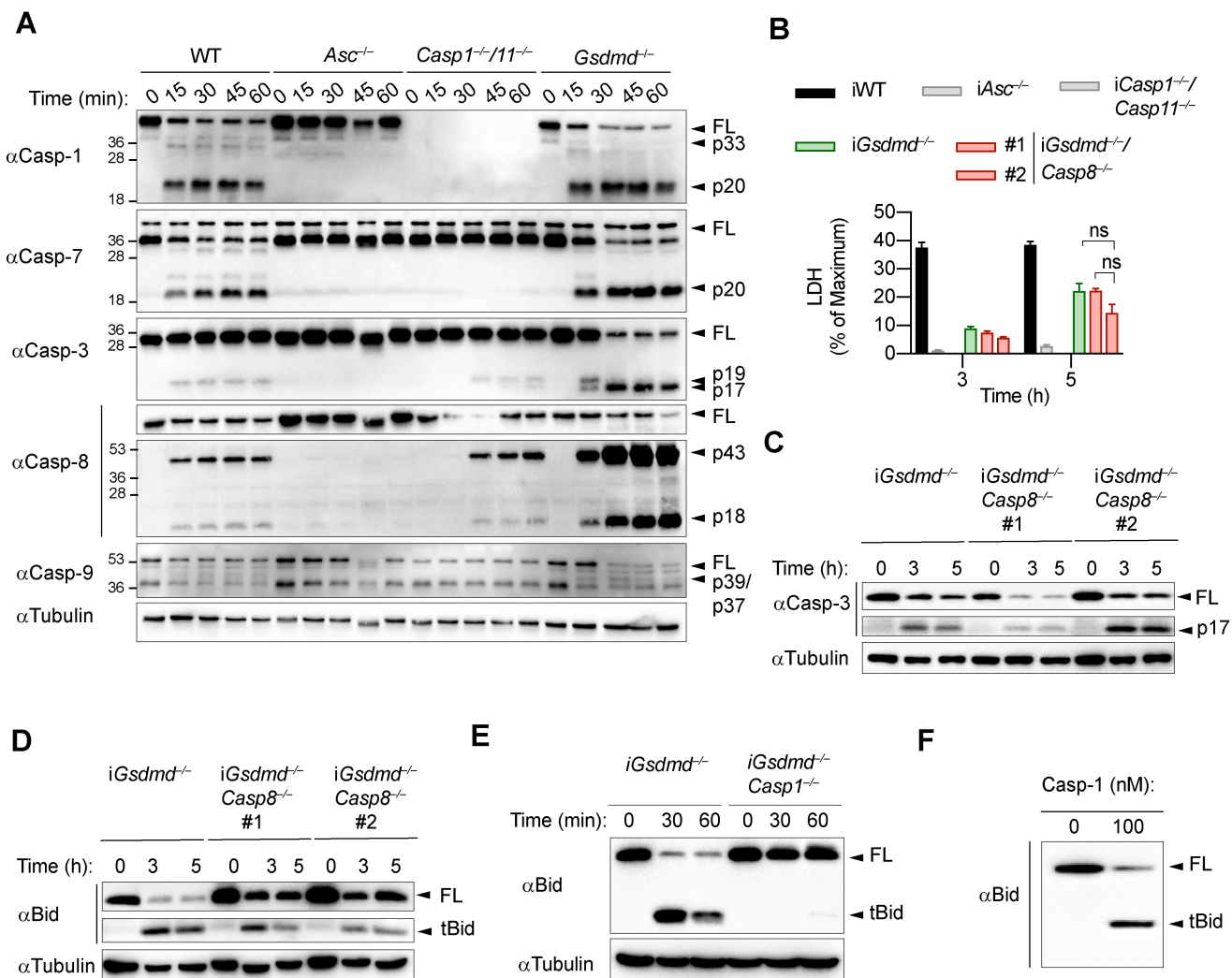


Figure 6

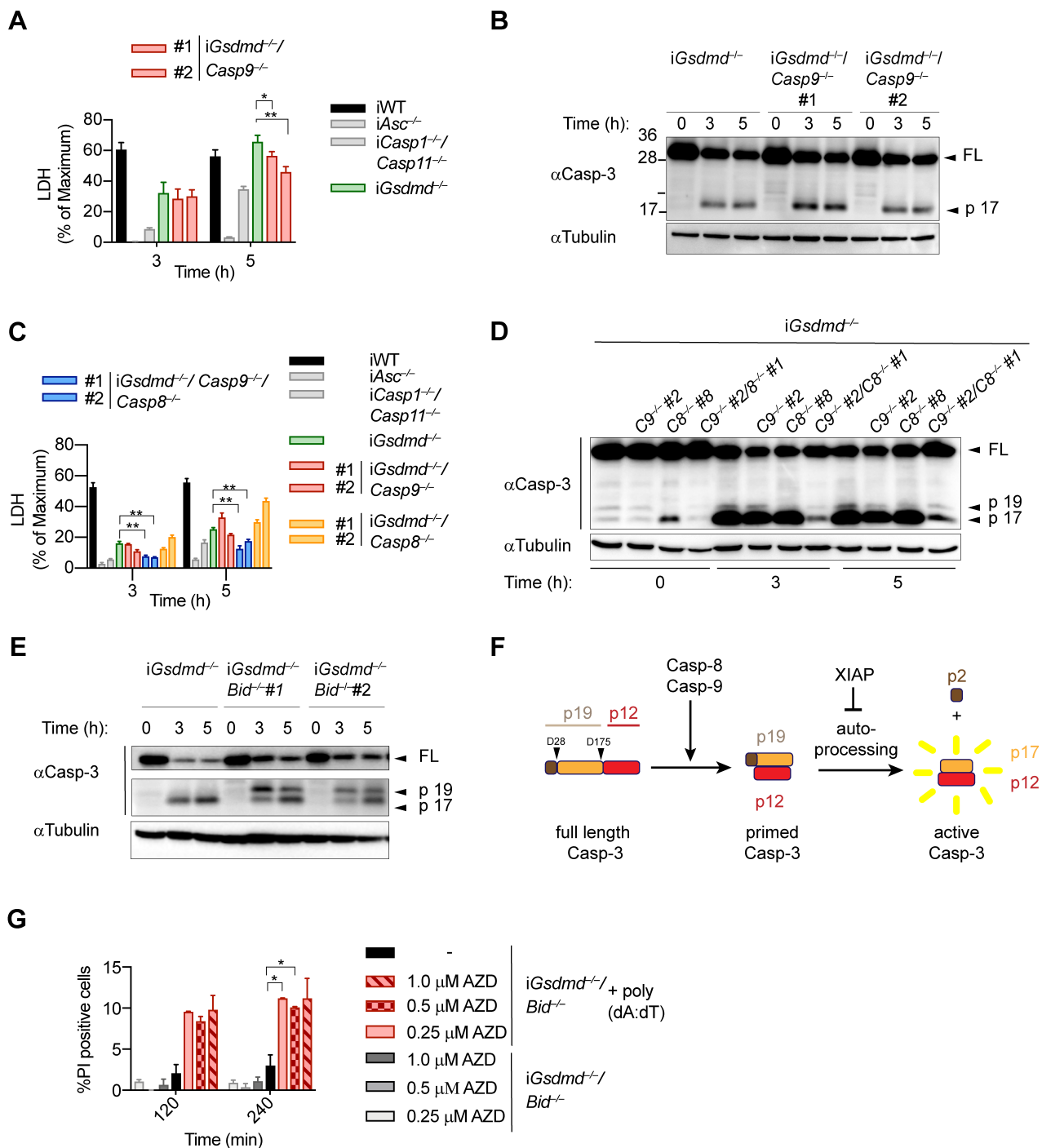


Figure 7

